Noncovalent Interactions of Cu^+ with *N*-Donor Ligands (Pyridine, 4,4-Dipyridyl, 2,2-Dipyridyl, and 1,10-Phenanthroline): Collision-Induced Dissociation and Theoretical Studies

N. S. Rannulu and M. T. Rodgers*

Department of Chemistry, Wayne State University, Detroit, Michigan 48202

Received: October 20, 2006; In Final Form: February 13, 2007

Collision-induced dissociation of complexes of Cu^+ bound to a variety of *N*-donor ligands (*N*-L) with Xe is studied using guided ion beam tandem mass spectrometry. The *N*-L ligands examined include pyridine, 4,4-dipyridyl, 2,2-dipyridyl, and 1,10-phenanthroline. In all cases, the primary and lowest-energy dissociation channel observed corresponds to the endothermic loss of a single intact *N*-L ligand. Sequential dissociation of additional *N*-L ligands is observed at elevated energies for the pyridine and 4,4-dipyridyl complexes containing more than one ligand. Ligand exchange processes to produce Cu^+Xe are also observed as minor reaction pathways in several systems. The primary cross section thresholds are interpreted to yield 0 and 298 K bond dissociation energies (BDEs) after accounting for the effects of multiple ion-neutral collisions, the kinetic and internal energy distributions of the reactants, and dissociation lifetimes. Density functional theory calculations at the B3LYP/6-31G* level are performed to obtain model structures, vibrational frequencies, and rotational constants for the neutral *N*-L ligands and the $Cu^+(N\text{-L})_x$ complexes. The relative stabilities of the various conformations of these *N*-L ligands and $Cu^+(N\text{-L})_x$ complexes as well as theoretical BDEs are determined from single point energy calculations at the B3LYP/6-311+G(2d,2p) level of theory using B3LYP/6-31G* optimized geometries. Excellent agreement between theory and experiment is observed for all complexes containing one or two *N*-L ligands, while theory systematically underestimates the strength of binding for complexes containing more than two *N*-L ligands. The ground-state structures of these complexes and the trends in the sequential BDEs are explained in terms of stabilization gained from sd-hybridization and repulsive ligand−ligand interactions. The nature of the binding interactions in the $Cu^+(N\text{-L})_x$ complexes are examined via natural bond orbital analyses.

Introduction

Transition metal complexes of *N*-donor heterocyclic ligands are important as a result of the many roles these complexes play in biological systems,[1−4] environmental issues,[5,6] electrochemical applications,[7] and supramolecular chemistry.[8,9] Transition and heavy metal ions play active roles in a variety of biological processes, being components of proteins, nucleic acids, vitamins, and drugs.[10] In all of these examples, the interactions between the transition metal ion and *N*-donor ligand(s) play a critical role in the biochemical processes that occur in organisms. For example, pyridine, a nitrogen containing heterocycle, is one of the most abundant and best known of the aromatic heterocyclic compounds widely distributed in nature, principally as enzymes and alkaloids. Pyridine is also used as a building block of many pharmaceuticals with different functionalities.[10]

Chelating ligands such as 2,2-dipyridyl and 1,10-phenanthroline are *N*-donor heterocyclic ligands extensively used in the synthesis of transition metal complexes, many of which are useful for a variety of biological applications. For example, the $Cu^+(1,10\text{-phenanthroline})_2$ complex is an efficient chemical nuclease that cleaves the phosphodiester backbone of both DNA and RNA under physiological conditions by oxidative attack of the deoxyribose moiety. Two roles of 1,10-phenanthroline in this reaction are important. First, it modulates the redox potential of the Cu^{2+}/Cu^+ couple. Second, it binds to DNA or RNA allowing the oxidative chemistry of the cuprous complex to proceed at the surface of the nucleic acid.[11−14] Derivatives of 2,2-dipyridyl also play influential roles in biological systems.[15] Their activities are usually a consequence of their ability to complex metal ions. Moreover, they are able to stimulate the activity of some enzymes, probably by removing metals that inhibit them.[16]

These chelating ligands are also employed for several interesting environmental applications. The need to remove highly toxic compounds from potential sources of drinking water with efficient catalytic materials is of profound importance. 2,2-dipyridyl and 1,10-phenanthroline are very good ligands for this purpose because they are capable of stabilizing both low and high valence species. The multiple binding sites of the ligand framework greatly stabilize metal−ligand complexes. Furthermore, these two ligands are extensively used to remove heavy metals from water due to their robust redox stability and ease of functionalization.[17,18]

The conjugated aromatic systems of 2,2-dipyridyl and 1,10-phenanthroline exhibit fluorescence that is drastically affected when metal ions bind to these ligands. Because the changes in florescence caused by chelation of metal ions are significant and detectable, these ligands have found applications as sensors for the detection of metal ions.[19−26] Ligands containing two or more 2,2-dipyridyl and 1,10-phenanthroline ligands can be used as bridges to interconnect metal centers in a well-

10.1021/jp066903h CCC: $37.00
Published on Web 04/18/2007

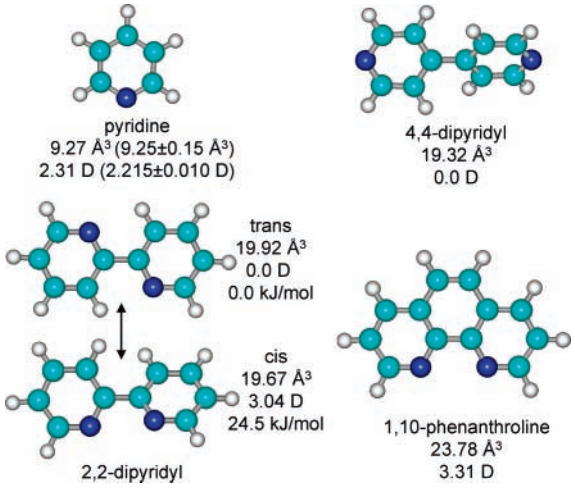

Figure 1. B3LYP/6-31G* optimized geometries of neutral pyridine, 4,4-dipyridyl, 2,2- dipyridyl, and 1,10-phenanthroline. Theoretical dipole moments and polarizabilities calculated here; experimental values are shown in parentheses (references 32−37).

defined spatial arrangement. Such ligands have been used as precursors for helical assembly,[27] chiral molecular recognition,[28,29] and other applications in photonics and optoelectronics.[30,31]

As a result of the widespread importance and applications of these chelating ligands it is desirable to better understand and quantitatively characterize the metal−ligand interactions in these complexes. Thus, in the current study, we examine the noncovalent interactions between Cu^+ and multiple ligands of pyridine ($x = 1-4$), 4,4-dipyridyl ($x = 1-4$), 2,2-dipyridyl ($x = 1-3$), and 1,10-phenanthroline ($x = 1-3$). Structures of these neutral *N*-donor ligands are shown in Figure 1 along with their calculated and measured dipole moments and molecular polarizabilities.[32−37] Collision-induced dissociation (CID) of these complexes is studied using guided ion beam tandem mass spectrometry techniques. The kinetic energy dependent cross sections for the CID processes are analyzed using methods developed previously.[38] The analysis explicitly includes the effects of the internal and translational energy distributions of the reactants, multiple ion-neutral collisions, and the lifetimes for dissociation. We derive $(N\text{-L})_{x-1}Cu^+-(N\text{-L})$ bond dissociation energies (BDEs) and compare these results to values obtained from density functional theory calculations performed here. Comparison of the binding interactions of monodentate ligands (pyridine and 4,4-dipyridyl) with chelating ligands (2,2-dipyridyl and 1,10-phenanthroline) is employed to gain a better understanding of the influence that the number and orientation of the donor atoms, and the size and flexibility of the ligands, has upon the binding interactions. Subsequently, trends in the sequential BDEs and total BDEs of these $Cu^+(N\text{-L})_x$ complexes provide a more detailed understanding of the binding in these systems.

Experimental Section

Experimental Protocol. The guided ion beam tandem mass spectrometer in which these experiments were performed has been described in detail elsewhere.[39] The $Cu^+(N\text{-L})_x$ complexes are formed by condensation of Cu^+, generated via dc discharge, with one or more neutral *N*-L ligands. These complexes are collisionally stabilized and thermalized by $>10^5$ collisions with the He and Ar bath gases, such that the internal energies of the complex ions are well described by a Maxwell−Boltzmann distribution at room temperature.[39] Ions are effusively sampled from the source, focused, accelerated, and focused into a magnetic sector momentum analyzer for reactant ion mass selection. The mass-selected ions are decelerated to a desired kinetic energy and injected into an octopole ion beam guide, which traps the ions in the radial direction. The octopole ion beam guide acts as an efficient radial ion trap such that loss of reactant and product ions as they drift through the octopole is almost entirely eliminated.[40,41] The octopole passes through a static gas cell containing Xe at a sufficiently low pressure (~0.05−0.20 mTorr) that multiple ion-neutral collisions are improbable. Unreacted beam and product ions drift to the end of the octopole and are focused into a quadrupole mass filter for mass analysis and subsequently detected with a secondary electron scintillation (Daly) detector using standard pulse counting techniques.

Data Handling. Ion intensities are converted to absolute cross sections using a Beer's law analysis as described previously.[42] Uncertainties in absolute cross sections are estimated to be ±20%, which are largely the result of errors in pressure measurement and uncertainties in the length of the interaction region. Relative uncertainties are approximately ±5%.

Ion kinetic energies in the laboratory frame, E_{lab}, are converted into energies in the center-of-mass frame, E_{cm}, using the formula $E_{cm} = E_{lab}m/(m+M)$, where M and m are the masses of the ionic and neutral reactants, respectively. All energies reported below are in the center-of-mass frame unless otherwise noted. The absolute zero and distribution of the ion kinetic energies are determined using the octopole ion guide as a retarding potential analyzer as previously described.[42] The distribution of ion kinetic energies is nearly Gaussian with a fwhm in the range from 0.3 to 0.4 eV (lab) for these experiments. The absolute uncertainty in the energy scale is ±0.05 eV.

Because multiple ion-neutral collisions can influence the shape of CID cross sections and the threshold regions are most sensitive to these effects, each CID cross section was measured twice at three nominal Xe pressures (0.05, 0.10, and 0.20 mTorr). Data free from pressure effects are obtained by extrapolating to zero reactant pressure, as described previously.[43] Thus, cross sections subjected to thermochemical analysis are due to single bimolecular encounters.

Theoretical Calculations. Density functional theory calculations were performed to obtain model structures, vibrational frequencies, rotational constants, and energetics for the neutral *N*-L ligands and $Cu^+(N\text{-L})_x$ complexes. Geometry optimizations and frequency analyses of the optimized structures were performed at the B3LYP/6-31G* level.[44,45] When used to model the data or to calculate thermal energy corrections, the B3LYP/6-31G* vibrational frequencies are scaled by a factor of 0.9804.[46] The scaled vibrational frequencies thus obtained for these systems are listed in the Supporting Information in Table 1S, while Table 2S lists the rotational constants. Single-point energy calculations were performed at the B3LYP/6-311+G(2d,2p) level using the B3LYP/6-31G* optimized geometries. Independent zero-point energy (ZPE) and basis set superposition error (BSSE) corrections are included in the calculated BDEs.[47,48] Transition states for the interconversion of *cis*- and *trans*-2,2-dipyridyl in the absence and in the presence of Cu^+ were calculated at the B3LYP/6-311+G(2d,2p) level using the B3LYP/6-31G* optimized geometries.

Isotropic molecular polarizabilities of the neutral *N*-L ligands (pyridine, 4,4-dipyridyl, *cis*- and *trans*-2,2-dipyridyl, and 1,10-phenanthroline) were calculated at the PBE0/6-311+G(2d,2p) level of theory using the B3LYP/6-31G* optimized geometries.

This level of theory has been shown to provide polarizabilities that are in good agreement with measured values.[49]

Natural bond orbital (NBO) analyses of the Cu^+(pyridine), Cu^+(4,4-dipyridyl), Cu^+(pyridine)$_2$, Cu^+(2,2-dipyridyl), and Cu^+(1,10-phenanthroline) complexes were performed to gain insight into the nature of the binding interactions in the $Cu^+(N\text{-L})_x$ complexes. The NBO program[50] in Gaussian 98 performs the analysis of many electron-molecular wave functions in terms of localized electron pair "bonding" units, provides all possible interactions between filled Lewis-type electron-donor NBOs with non-Lewis electron-acceptor NBOs, and estimates the stabilization energy associated with the electron donor−acceptor interactions, $E(2)$ using second-order perturbation theory. The NBO analyses were performed at the B3LYP/6-311+G(2d2,p) level of theory using the B3LYP/6-31G* geometry optimized structures.

Thermochemical Analysis. The threshold regions of the CID reaction cross sections are modeled using eq 1:

$$\sigma(E) = \sigma_0 \sum_i g_i (E + E_i - E_0)^n / E \qquad (1)$$

where σ_0 is an energy-independent scaling factor, E is the relative kinetic energy of the reactants, E_0 is the threshold for reaction of the ground electronic and ro−vibrational state, and n is an adjustable parameter that describes the efficiency of kinetic to internal energy transfer.[51] The summation is over the ro−vibrational states of the reactant ions, i, having energies, E_i, and populations, g_i, where $\Sigma g_i = 1$. We assume that the relative reactivity, as reflected by σ_0 and n, is the same for all ro−vibrational states.

The Beyer−Swinehart algorithm[52] is used to determine the density of ro-vibrational states, and the relative populations, g_i, are calculated for a Maxwell−Boltzmann distribution at 298 K, the internal temperature of the reactants. The vibrational frequencies are determined from electronic structure calculations as discussed in the Theoretical Calculations section. The average vibrational energy at 298 K of the neutral *N*-L ligands and $Cu^+(N\text{-L})_x$ complexes is given in the Supporting Information in Table 1S. We have increased and decreased the prescaled vibrational frequencies (0.9804) by 10% as an estimate of one standard deviation in the uncertainty in the vibrational energy (Table 1S).

The dissociation of ions is expected to become slower as the size of the reactant ions increases and the strength of the metal−ligand interaction increases. This leads to an increased probability that dissociation does not occur on the experimental time scale, $\sim 10^{-4}$ s for the experiments performed here. All CID processes faster than this are observed. However, as the lifetime of the energized molecule approaches this limit, the apparent CID threshold shifts to higher energies, a so-called kinetic shift. This kinetic shift is quantified and corrected for in our analysis by including statistical theories for unimolecular dissociation, specifically Rice−Ramsperger−Kassel−Marcus (RRKM) theory, into eq 1 as described in detail elsewhere.[38,53] This requires sets of ro−vibrational frequencies appropriate for the energized molecules and the transition states (TSs) leading to dissociation. A loose phase space limit (PSL) TS model[38] is used because the interaction between Cu^+ and these *N*-L ligands is largely electrostatic. The molecular parameters of the EM and TS are provided in the Supporting Information in Tables 1S and 2S.

Equation 1 is convoluted with the kinetic and internal energy distributions of the reactants and a nonlinear least-squares analysis of the data is performed to give optimized values for the parameters σ_0, E_0, or E_0(PSL), and n.[42] Uncertainties in E_0 and E_0(PSL) are determined from the range of threshold values for the eight zero-pressure-extrapolated data sets, variations associated with the vibrational frequencies (scaling as discussed above), and the error in the absolute energy scale, 0.05 eV (lab). For analyses that include the RRKM lifetime analysis, the uncertainties in the reported E_0(PSL) values also include the effects of increasing and decreasing the time assumed available for dissociation by a factor of 2.

Equation 1 explicitly includes the internal energy of the reactant ion, E_i. All energy available is treated statistically because the ro-vibrational energy of the reactants is redistributed throughout the ion upon impact with the collision gas, Xe. The threshold energies for dissociation reactions determined by analysis with eq 1 are equated to 0 K BDEs, which should be valid for the simple noncovalent bond cleavage reactions examined here.[43,54]

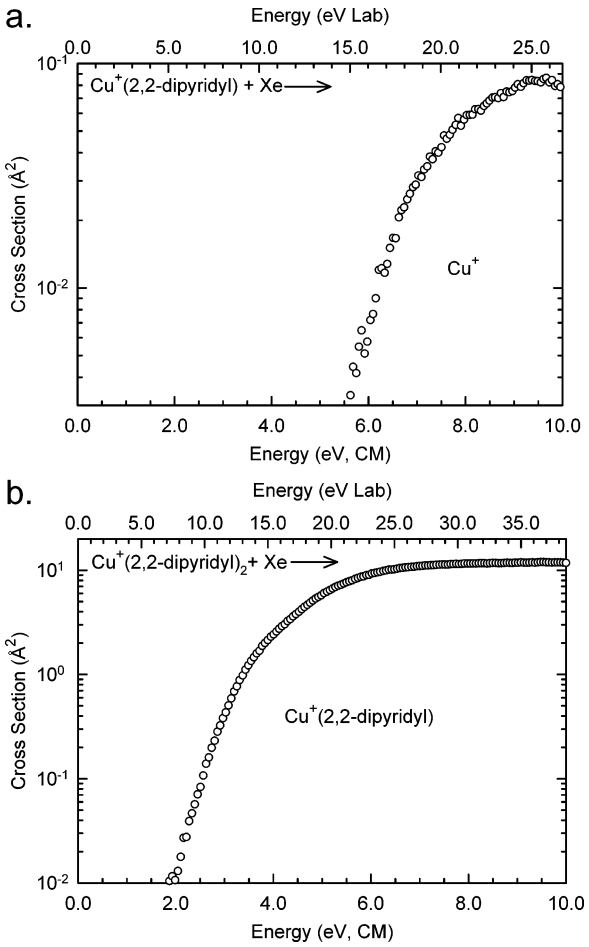

Figure 2. Cross sections for collision-induced dissociation of Cu^+(2,2-dipyridyl)$_x$ complexes, $x = 1$ and 2 for parts a and b, respectively, with Xe as a function of kinetic energy in the center-of-mass frame (lower *x*-axis) and laboratory frame (upper *x*-axis). Data are shown for a Xe pressure of ~0.2 m Torr.

Results

Cross Sections for Collision-Induced Dissociation. Experimental cross sections were obtained for the interaction of Xe with 11 $Cu^+(N\text{-L})_x$ complexes, where *N*-L = pyridine (x = 1−4), 4,4-dipyridyl (x = 1−3), 2,2-dipyridyl (x = 1−2), and 1,10-phenanthroline (x = 1−2). Figure 2 shows representative data for the Cu^+(2,2-dipyridyl)$_x$ complexes. The other $Cu^+(N\text{-L})_x$ complexes exhibit similar behavior and are shown in the Supporting Information as Figure 1S. The sequential loss of intact *N*-L ligands and ligand exchange with Xe are the only

processes observed in these systems over the energy range examined, ~0−10 eV. The most favorable process for all complexes is the loss of a single intact neutral *N*-L ligand in the CID reactions 2:

$$Cu^+(N\text{-L})_x + Xe \rightarrow Cu^+(N\text{-L})_{x-1} + N\text{-L} + Xe \qquad (2)$$

At elevated energies dissociation of additional *N*-L ligands is observed for the more highly ligated $Cu^+(pyridine)_x$ and $Cu^+(4,4\text{-dipyridyl})_x$ complexes, i.e., $x \geq 2$. The shapes of the CID cross sections confirm that these products are formed sequentially from the primary $Cu^+(N\text{-L})_{x-1}$ product, i.e., the cross section for formation of $Cu^+(N\text{-L})_{x-1}$ begins to decline as the cross section for the secondary product, $Cu^+(N\text{-L})_{x-2}$, begins to appear. Similar behavior is also observed for the higher order dissociation processes. Ligand exchange to form Cu^+Xe is observed in the Cu^+(pyridine) and Cu^+(4,4-dipyridyl) systems. It is likely that this process occurs for all complexes, but that the signal-to-noise in other experiments was not sufficient to differentiate the Cu^+Xe product from background noise.

Cu^+(Pyridine)$_x$. The CID behavior of the $Cu^+(pyridine)_x$ complexes is shown in the Supporting Information, Figure 1S parts a−d. Cu^+(pyridine) dissociates via loss of pyridine to produce Cu^+ at an apparent threshold near 2.0 eV and a maximum cross section of ~1.2 Å^2. The ligand exchange product Cu^+Xe is observed at an apparent threshold of 2.6 eV; its cross section drops off rapidly with energy due to competition with the primary CID process. $Cu^+(pyridine)_2$ dissociates via loss of a single pyridine molecule at an apparent threshold near 2.0 eV and a maximum cross section of ~12 Å^2. Loss of a second pyridine molecule to produce Cu^+ is observed at elevated energies with an apparent threshold near 6.0 eV, but accounts for less than 1% of the observed dissociation. The CID behavior of $Cu^+(pyridine)_3$ is notably different, loss of the first pyridine molecule begins at an apparent threshold near or below 0 eV with a much larger cross section magnitude, ~75 Å^2. The threshold for the secondary Cu^+(pyridine) product appears near 2.2 eV with a maximum cross section of ~5 Å^2. Complete dissociation to produce Cu^+ is not observed over the collision range examined. The CID behavior of $Cu^+(pyridine)_4$ is similar to that observed for $Cu^+(pyridine)_3$, except that the magnitude of the secondary $Cu^+(pyridine)_2$ product cross section is larger than the primary $Cu^+(pyridine)_3$ product cross section at energies beyond 3 eV. The apparent threshold for the primary product $Cu^+(pyridine)_3$ appears near 0 eV with a cross section magnitude of ~75 Å^2, similar to the behavior observed for the triply ligated system. The cross section for production of the primary product, $Cu^+(pyridine)_3$, decreases more rapidly than observed for the triply ligated species beginning at the apparent threshold for the $Cu^+(pyridine)_2$ product. The $Cu^+(pyridine)_2$ product also exhibits an apparent threshold near 0 eV and a maximum cross section magnitude of ~50 Å^2. The apparent threshold for the Cu^+(pyridine) product occurs near 2.5 eV and reaches a maximum cross section of ~1 Å^2. As the extent of ligation increases, the primary cross section declines more rapidly at elevated energies because of the increasing number of pathways available for decomposition of the primary products.

Cu^+(4,4-Dipyridyl)$_x$. The CID behavior observed for the $Cu^+(4,4\text{-dipyridyl})_x$ complexes is quite similar to that observed for the $Cu^+(pyridine)_x$ complexes, except that the apparent thresholds of the analogous pathways are shifted to slightly higher energies. This apparent shift to higher energies arises as a result of the larger number of vibrational modes in these complexes that lead to a reduction in the rate of unimolecular dissociation. The cross section magnitudes are slightly smaller for the $x = 1$ and 2 complexes, ~0.6 and ~10.0 Å^2, but is substantially larger for the $Cu^+(4,4\text{-dipyridyl})_3$ complex, ~200 Å^2, as compared to the analogous $Cu^+(pyridine)_x$ systems.

Cu^+(2,2-Dipyridyl)$_x$. The CID behavior for the interaction of the $Cu^+(2,2\text{-dipyridyl})_x$ complexes with Xe is notably different from that observed for the monodentate ligands with respect to the apparent threshold and the magnitude of the cross section. The loss of 2,2-dipyridyl from Cu^+(2,2-dipyridyl) begins at an apparent threshold near 6.0 eV and exhibits a maximum cross section of ~0.08 Å^2. The ligand exchange product Cu^+Xe is not observed or cannot be differentiated from background noise. Interaction of $Cu^+(2,2\text{-dipyridyl})_2$ with Xe results in loss of a single 2,2-dipyridyl ligand at an apparent threshold near 2.0 eV and a maximum cross section of ~10.0 Å^2. Sequential dissociation to produce bare Cu^+ was not observed over the range of collision energies examined.

Cu^+(1,10-Phenanthroline)$_x$. The CID behavior observed for the $Cu^+(1,10\text{-phenanthroline})_x$ complexes is remarkably similar to that observed for the $Cu^+(2,2\text{-dipyridyl})_x$ systems, except that the apparent thresholds are shifted to slightly higher energies. Again, this shift to higher energies results from the increased number of modes available to these systems. The cross section magnitudes are also slightly larger, ~0.1 Å^2 for the $x = 1$ and ~14 Å^2 for the $x = 2$ complexes, which is likely the result of the larger size and polarizability of this ligand.

Threshold Analysis. The threshold regions for reactions 2 in 11 $Cu^+(N\text{-L})_x$ complexes were analyzed using the model of eq 1. In general, the analysis of the primary CID threshold provides the most reliable thermochemistry because sequential dissociation products are more sensitive to lifetime effects,[43,53] and additional assumptions are needed to quantitatively include the multiple products formed. Good reproduction of the data is obtained over energy ranges exceeding 6 eV for the $Cu^+(N\text{-L})_x$ complexes, where $x = 1$ and 2. The zero-pressure-extrapolated CID cross sections and fits to the data using a loose PSL model for the interaction of $Cu^+(2,2\text{-dipyridyl})_x$, where $x = 1$ and 2, with Xe are shown in Figure 3. As can be seen in the figure, the cross sections are accurately reproduced using a loose PSL TS model. Previous work has shown that this model provides the most accurate assessment of the kinetic shifts for CID processes of electrostatically bound ion−molecule complexes.[55−57,67]

For the $Cu^+(N\text{-L})_x$ complexes where $x = 3$ and 4, sequential dissociation processes lead to a high-energy fall off in the primary product cross section that decreases the range over which the data can be reproduced to ~2 eV. Because the high-energy fall off narrows the fitting range of the cross section, the analyses must include the effects of subsequent ligand loss. This is achieved by using a simple statistical model that conserves angular momentum, as described in detail previously.[58] This model depends on E_D, the energy at which the sequential dissociation channel begins, and p, a parameter similar to n in eq 1. This extended model was employed for the analyses of the $Cu^+(pyridine)_3$, $Cu^+(pyridine)_4$, and $Cu^+(4,4\text{ dipyridyl})_3$ complexes. Analyses of the total CID cross sections using a loose PSL TS model were also performed for these systems. Although the high-energy model has proven to be extremely useful in describing such subsequent dissociations, lifetime effects have not been incorporated in the model. Because such effects could be appreciable in these rather large complexes, the reliability of the analyses that include this simple high-energy model is unclear. Therefore, we believe that the results obtained by reproducing the total cross sections for the $Cu^+(pyridine)_3$,

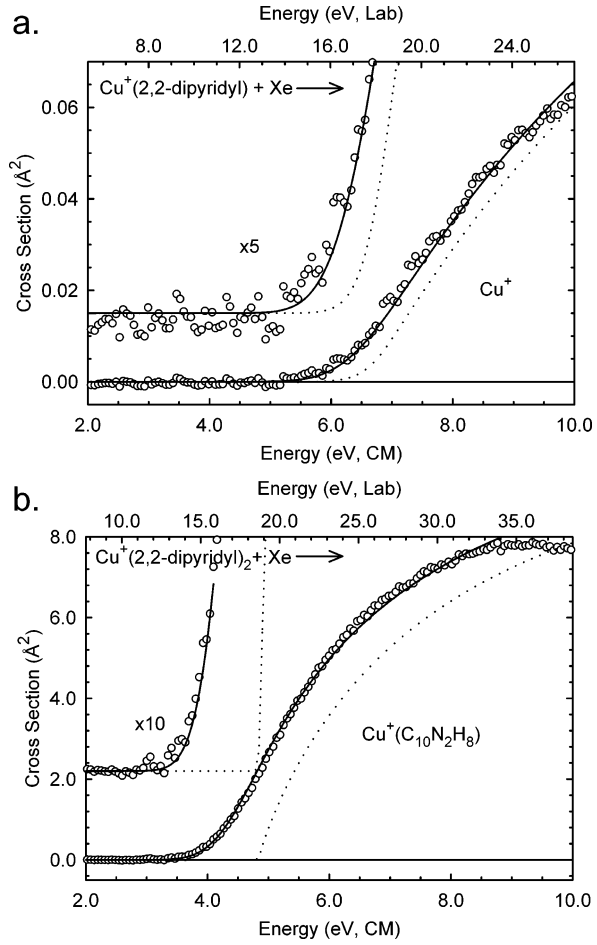

Figure 3. Zero-pressure extrapolated cross sections for collision-induced dissociation of $Cu^+(2,2\text{-dipyridyl})_x$ complexes, $x = 1$ and 2 for parts a and b, respectively, with Xe in the threshold region as a function of kinetic energy in the center-of-mass frame (lower *x*-axis) and laboratory frame (upper *x*-axis). Solid lines show the best fits to the data using eq 1 convoluted over the ion kinetic and internal energy distributions. Dashed lines show the model cross section in the absence of experimental kinetic energy broadening for reactants with an internal energy corresponding to 0 K.

$Cu^+(pyridine)_4$, and $Cu^+(4,4\text{- dipyridyl})_3$ complexes are probably the most reliable. The results of these analyses are provided in Table 1.

Kinetic Shifts. Two threshold values E_0 and E_0(PSL) are listed in Table 1 for each complex. E_0 represents the threshold obtained for analyses that do not include RRKM lifetime effects, while E_0(PSL) represents the threshold obtained when the RRKM lifetime analysis is included. The difference in the E_0 and E_0(PSL) thresholds provides a measure of the kinetic shift associated with the finite time scale of our measurements. The total number of vibrational modes increases as the size of the complex increases. Similarly, the number of heavy atoms increases with the extent of ligation. Therefore, the density of states of the dissociating complexes increases with size. The density of states also increases with energy. Thus, the observed kinetic shifts should directly correlate with the size of the complex and the threshold energy.

$Cu^+(Pyridine)_x$. The measured BDEs for the $Cu^+(pyridine)_x$ complexes are 2.72, 2.45, 0.85, and 0.62 eV, while the kinetic shifts observed for these systems are 0.29, 0.88, 0.10, and 0.31 eV, for the $x = 1-4$ complexes, respectively. The total number of vibrations increases with the size of the complex from 36 for $Cu^+(pyridine)$ to 135 for $Cu^+(pyridine)_4$. Likewise, the number of heavy atoms increases form 7 to 25 as the size of the complex increases from one to four pyridine ligands. Because of the very strong binding interaction as compared to the $x = 3$ and 4 complexes and the larger number of modes relative to $Cu^+(pyridine)$, $Cu^+(pyridine)_2$ exhibits the largest kinetic shift among the $Cu^+(pyridine)_x$ systems examined here. The kinetic shift observed for $Cu^+(pyridine)_3$ is much smaller than that found for the other $Cu^+(pyridine)_x$ systems as a result of the much weaker binding as compared to the $x = 1$ and 2 complexes, and the smaller number of vibrational modes as compared to the $Cu^+(pyridine)_4$ complex.

$Cu^+(4,4\text{-Dipyridyl})_x$. The measured BDEs for the $Cu^+(4,4\text{-dipyridyl})_x$ complexes are 2.73, 2.41, and 0.66 eV, while the kinetic shifts observed for these systems are 1.56, 2.22, and 0.57 eV, for the $x = 1-3$ complexes, respectively. In the $Cu^+(4,4\text{ dipyridyl})_x$ complexes, the total number of vibrations increases from 63 for $Cu^+(4,4\text{ dipyridyl})$ to 183 for $Cu^+(4,4\text{ dipyridyl})_3$, while the number of heavy atoms increases from 13 to 37. Because of the similarities in the nature of the binding interactions, and the larger number of vibrational modes relative to $Cu^+(pyridine)_x$ complexes, the $Cu^+(4,4\text{-dipyridyl})_x$ complexes exhibit kinetic shifts that parallel those of the $Cu^+(pyridine)_x$ complexes, but are larger in magnitude.

$Cu^+(2,2\text{-Dipyridyl})_x$. The measured BDEs for the $Cu^+(2,2\text{-dipyridyl})_x$ complexes are 3.84 and 2.46 eV, while the corresponding kinetic shifts are 2.68 and 2.14 eV, for the $x = 1$ and 2 complexes, respectively. The total number of vibrations increases from 63 for $Cu^+(2,2\text{-dipyridyl})$ to 123 for $Cu^+(2,2\text{-dipyridyl})_2$. Likewise, the number of heavy atoms increases from 13 to 25 as the size of the cluster increases from one to two 2,2-dipyridyl ligands. Because of the very strong binding interactions relative to the corresponding $Cu^+(pyridine)_x$ and $Cu^+(4,4\text{-dipyridyl})_x$ complexes, and the larger number of vibrational modes, the $Cu^+(2,2\text{-dipyridyl})_x$ complexes exhibit much larger kinetic shifts.

$Cu^+(1,10\text{-Phenanthroline})_x$. The measured BDEs for the $Cu^+(1,10\text{-phenanthroline})_x$ complexes are 4.09 and 2.42 eV, while the kinetic shifts observed for these systems are 3.30 and 2.02 eV, for the $x = 1$ and 2 complexes, respectively. In the $Cu^+(1,10\text{-phenanthroline})_x$ systems, the total number of vibrations varies from 69 to 135 and the number of heavy atoms varies from 15 to 29 as the size of the complex increases from one to two 1,10-phenanthroline ligands. Of the $Cu^+(N\text{-L})_x$ complexes examined here, the largest kinetic shift is observed for $Cu^+(1,10\text{-phenanthroline})$, consistent with it exhibiting the strongest binding interaction, Table 1. The trends in the kinetic shifts for the $Cu^+(2,2\text{-dipyridyl})_x$ and $Cu^+(1,10\text{-phenanthroline})_x$ complexes indicate that the much stronger binding in the mono-complexes leads to slower unimolecular dissociation than the increased number of vibrational modes present in the bis-complexes.

The entropy of activation, $\Delta S^\dagger$, provides a measure of the looseness of the TS and is also a reflection of the complexity of the system. It is determined from the molecular parameters used to model the energized molecule and TS for dissociation, but also depends upon the threshold energy. Listed in Table 1, the $\Delta S^\dagger$(PSL) values at 1000 K vary between 35 and 85 J K^{-1} mol^{-1} for the $Cu^+(N\text{-L})_x$ complexes examined here. The entropies increase with the size of the complex, i.e., as *x* increases for a given *N*-L ligand, and for a fixed value of *x* as the size of the *N*-L ligand increases. $\Delta S^\dagger$ is also larger for the chelating ligands than for the monodentate ligands as a result of the stronger and more geometrically constrained binding in the metal-chelate complexes.

TABLE 1: Fitting Parameters of Eq 1, Threshold Dissociation Energies at 0 K, and Entropies of Activation at 1000 K of Cu^+ (N-L)$_x$ Complexes

species	σ_0[a]	n[b]	E_0[c] (eV)	E_0 (PSL)[b] (eV)	kinetic shift (eV)	ΔS (PSL) (J K^{-1} mol^{-1})
Cu^+(pyridine)	1.4 (0.1)	1.1 (0.1)	3.01 (0.02)	2.72 (0.08)	0.29	40.0 (2.0)
Cu^+(pyridine)$_2$	8.5 (0.5)	1.6 (0.1)	3.33 (0.04)	2.45 (0.09)	0.88	55.2 (4.0)
Cu^+(pyridine)$_3$	114.2 (3.6)[d]	0.7 (0.1)[d]	0.95 (0.02)[d]	0.85 (0.02)[d]	0.10[d]	66.7 (4.0)[d]
	111.9 (3.1)[e]	0.7 (0.1)[e]	0.95 (0.02)[e]	0.85 (0.02)[e]	0.10[e]	66.7 (4.0)[e]
Cu^+(pyridine)$_4$	100.7 (3.7)[d]	1.0 (0.1)[d]	0.99 (0.01)[d]	0.69 (0.05)[d]	0.30[d]	53.4 (5.0)[d]
	79.8 (2.6)[e]	0.9 (0.1)[e]	0.93 (0.01)[e]	0.62 (0.03)[e]	0.31[e]	54.4 (5.0)[e]
Cu^+(4,4-dipyridyl)	0.7 (0.1)	1.4 (0.1)	4.29 (0.16)	2.73 (0.11)	1.56	35.2 (2.0)
Cu^+(4,4-dipyridyl)$_2$	6.7 (0.5)	1.7 (0.1)	4.63 (0.06)	2.41 (0.07)	2.22	49.7 (4.0)
Cu^+(4,4-dipyridyl)$_3$	225.8 (8.7)[d]	1.0 (0.1)[d]	1.23 (0.01)[d]	0.66 (0.02)[d]	0.57[d]	71.2 (4.0)[d]
	225.8 (8.7)[e]	1.0 (0.1)[e]	1.23 (0.01)[e]	0.66 (0.02)[e]	0.57[e]	71.2 (4.0)[f]
Cu^+(2,2-dipyridyl)	0.2 (0.1)	1.0 (0.1)	6.52 (0.13)	3.84 (0.05)	2.68	53.4 (2.0)
Cu^+(2,2-dipyridyl)$_2$	28.5 (0.4)	0.9 (0.1)	4.60 (0.04)	2.46 (0.10)	2.14	84.3 (4.0)
Cu^+(1,10-phenanthroline)	0.6 (0.1)	0.6 (0.1)	7.39 (0.06)	4.09 (0.13)	3.30	61.0 (2.0)
Cu^+(1,10-phenanthroline)$_2$	11.3 (7.9)	1.6 (0.4)	4.44 (0.18)	2.42 (0.04)	2.02	85.0 (5.0)

[a] Uncertainties are listed in parentheses. [b] Average values for a loose PSL transition state. [c] No RRKM analysis. [d] Average values obtained for fits to the primary product cross section. [e] Average values obtained for fits to the total cross section.

TABLE 2: Bond Dissociation Energies of Cu^+ (N-L)$_x$ Complexes at 0 K in kJ/mol

	experiment			theory			
complex	TCID[a]	literature[b]	total BDE[g]	D_e[d]	D_0[d,e]	$D_{0,BSSE}$[d,f]	total BDE[i]
Cu^+(pyridine)	262.3 (7.7)	245.9 (10.1)[h] 274.1 (75.2)[i]	262.3 (7.7)	269. 9	264. 0	262.0	262.0
Cu^+(pyridine)$_2$	236.3 (8.7)		498.6 (11.6)	247. 7	241. 3	238.9	500.9
Cu^+(pyridine)$_3$	82.4 (2.2)		581.0 (11.8)	53.2	51.2	48.8	549.7
Cu^+(pyridine)$_4$	60.2 (2.6)		641.2 (12.1)	44.2	40.2	37.3	587.0
Cu^+(4,4-dipyridyl)	263.7 (10.6)		263.7 (10.6)	270. 0	265. 1	263.1	263.1
Cu^+(4,4-dipyridyl)$_2$	232.8 (7.0)		496.5 (12.7)	242. 8	237. 4	226.4	489.5
Cu^+(4,4-dipyridyl)$_3$	63.4 (1.6)		559.9 (12.8)	46.5	39.5	34.9	524.4
Cu^+(4,4-dipyridyl)$_4$			38.2	35.6	32.8	557.2	
Cu^+(2,2-dipyridyl)	370.3 (12.9)		370.3 (12.9)	368. 5	362. 3	358.9	358.9
Cu^+(2,2-dipyridyl)$_2$	237.7 (9.7)		608.0 (16.1)	235. 4	230. 0	227.0	585.9
Cu^+(2,2-dipyridyl)$_3$				−40. 2	−41. 8	−46.9	
Cu^+(1,10-phenanthroline)	395.0 (12.5)		395.0 (12.5)	403. 2	396. 4	393.2	393.2
Cu^+(1,10-phenanthroline)$_2$	233.0 (4.1)		628.0 (13.2)	241. 1	234. 3	229.2	622.4
Cu^+(1,10-phenanthroline)$_3$				3.0	1.7	−3.7	

[a] Present results, threshold collision-induced dissociation (TCID). [b] All literature values adjusted to 0 K. [c] Total BDE of the complex. [d] Calculated at the B3LYP/6-311+G(2d,2p) level of theory using B3LYP/6-31G* optimized geometries. [e] Including ZPE corrections with B3LYP/6-31G* frequencies scaled by 0.9804. [f] Also includes BSSE corrections. [g] Total theoretical BDE including ZPE and BSSE corrections. [h] Reference 60, TCID. [i] Reference 66, photodissociation.

Theoretical Results. Optimized geometries for the neutral N-L ligands and Cu^+ (N- L)$_x$ complexes were calculated using Gaussian 98 as described in the Theoretical Calculations section. Calculated BDEs determined at the B3LYP/6-311+G(2d,2p)// B3LYP/6-31G* level of theory are listed in Table 2. Independent ZPE and BSSE corrections are made for all complexes. The B3LYP/6-31G* optimized structures of the neutral N-L ligands along with their measured and calculated dipole moments and isotropic molecular polarizabilities are shown in Figure 1.

The calculated dipole moments of these N-L ligands vary considerably. The dipole moment of pyridine is calculated to be 2.31 D. This value is somewhat larger than the measured value, 2.215 ± 0.010 D,[32] suggesting that the dipole moments calculated here for the other N-L ligands may be slightly overestimated. Each of the pyridyl rings of 4,4-dipyridyl are expected to exhibit local dipole moments similar to that of pyridine. However, symmetry leads to cancellation of the local dipoles, and therefore 4,4-dipyridyl exhibits no net dipole moment. Similarly, the local dipole moments of the pyridyl rings of 2,2-dipyridyl cancel in the ground-state trans-conformer resulting in no net dipole moment, but reinforce to produce a large dipole moment of 3.04 D for the cis-conformer. The more extensive π network of 1,10-phenanthroline, as compared to 2,2-dipyridyl, leads to a modest increase in the dipole moment, 3.31 D.

The calculated isotropic molecular polarizabilities of these N-L ligands depend largely on the size of the ligand, but also exhibit a minor dependence on conformation. Pyridine, the smallest ligand has a calculated polarizability of 9.27 Å^3. This value is in excellent agreement with the measured polarizability of pyridine, 9.25 ± 0.15 Å^3.[33−37] The polarizabilities of the dipyridyl ligands are calculated to be slightly more than twice as large, 19.32, 19.67, and 19.92 Å^3 for the 4,4-dipyridyl, cis-2,2-dipyridyl, and trans-2,2-dipyridyl conformers, respectively. As previously suggested, the molecular polarizability only exhibits a slight dependence on conformation.[59] The polarizability of 1,10-phenanthroline is the largest of all of the N-L ligands examined here, 23.78 Å^3, in accord with it being the largest of these N-L ligands.

The B3LYP/6-31G* optimized geometries for the Cu^+(pyridine)$_x$, Cu^+(4,4-dipyridyl)$_x$, Cu^+(2,2-dipyridyl)$_x$, and Cu^+(1,10-phenanthroline)$_x$ complexes are shown in Figures 4−7, respectively. Key geometrical parameters of the optimized structures for each of these species are summarized in Table 3.

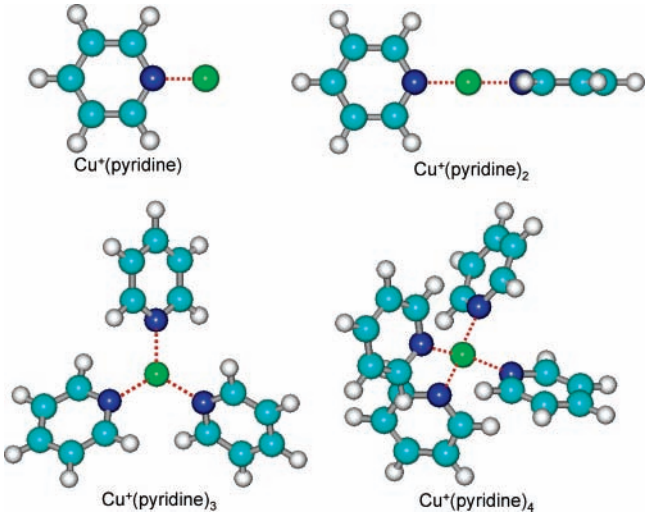

Figure 4. B3LYP/6-31G* optimized geometries of $Cu^+(pyridine)_x$, $x = 1-4$. Relative energies determined at the B3LYP/6-311+G(2d,2p) level of theory including ZPE corrections.

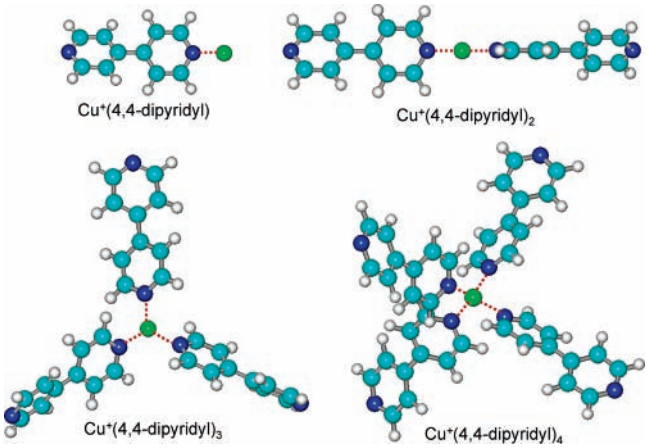

Figure 5. B3LYP/6-31G* optimized geometries of $Cu^+(4,4\text{-dipyridyl})_x$, $x = 1-4$. Relative energies determined at the B3LYP/6-311+G(2d,-2p) level of theory including ZPE corrections.

The theoretical calculations find that in all of these complexes, Cu^+ prefers to bind to the lone pair(s) of electrons on the nitrogen atoms rather than the π cloud of the aromatic ring(s). This preference for metal cation binding to the lone pair of electrons on the nitrogen atom(s) over binding to the π cloud was previously observed for a wide variety of aromatic *N*-L ligands.[56,60−63]

$Cu^+(Pyridine)_x$. Stable structures are found for the $Cu^+(pyridine)_x$ complexes in which the arrangement of the N atoms of the pyridine ligands around Cu^+ approaches the ideal structures predicted by the valence shell electron pair repulsion (VSEPR) model, i.e., a linear for $x = 1$ and 2, trigonal planar for $x = 3$, and tetrahedral for $x = 4$.[64] The distortion of the pyridine ligand(s) that occurs upon binding to Cu^+ is minor. The change in geometry is largest for the smallest complex, Cu^+(pyridine), and decreases with increasing ligation. The Cu^+-N bond lengths increase from 1.785 to 2.016 Å as the number of pyridine ligands around Cu^+ increases from one to four as a result of increasing ligand−ligand repulsion (Table 3).

$Cu^+(4,4\text{-Dipyridyl})_x$. Similar binding geometries to those found for the $Cu^+(pyridine)_x$ complexes are found for the $Cu^+(4,4\text{-dipyridyl})_x$ complexes. However, in neutral 4,4-dipyridyl, the pyridyl moieties are twisted with respect to each other by 36.2° to minimize repulsion between the hydrogen atoms of the adjacent pyridyl rings. Upon binding to Cu^+, the dihedral angle between the two pyridyl moieties of the 4,4-dipyridyl ligand reduces to 32.8° as a result of donation of electron density to Cu^+ thereby decreasing the electron density on the ligand. The dihedral angle between the two pyridyl moieties of the 4,4-dipyridyl ligands increases slightly with increasing ligation (Table 3). The Cu^+-N bond lengths are very similar to those in the $Cu^+(pyridine)_x$ complexes and increase from 1.780 to 2.018 Å as the number of 4,4-dipyridyl ligands

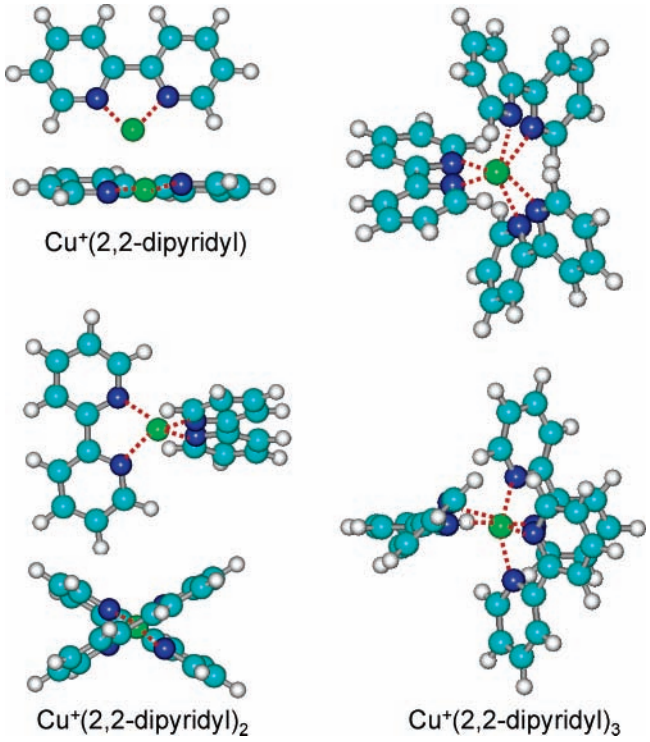

Figure 6. B3LYP/6-31G* optimized geometries of Cu^+ $(2,2\text{-dipyridyl})_x$, $x = 1-3$. Relative energies determined at the B3LYP/6-311+G-(2d,2p) level of theory including ZPE corrections.

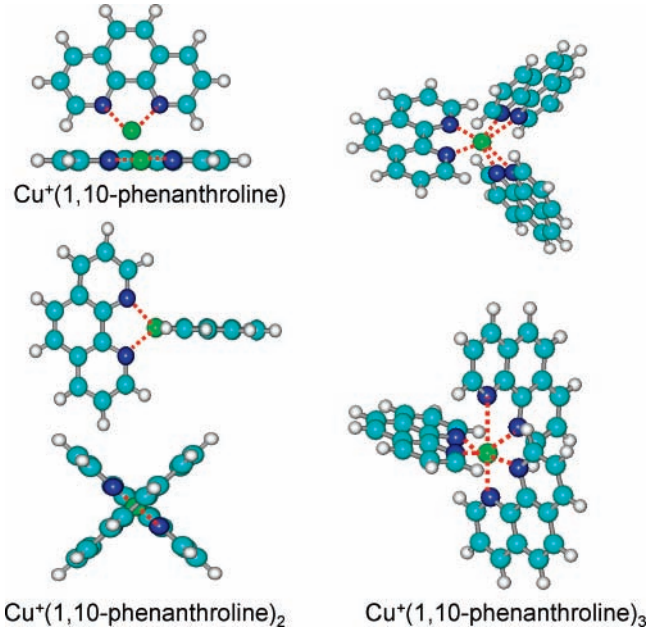

Figure 7. B3LYP/6-31G* optimized geometries of $Cu^+(1,10\text{-phenanthroline})_x$, $x = 1-3$. Relative energies determined at the B3LYP/6-311+G(2d,2p) level of theory including ZPE corrections.

TABLE 3: Geometrical Parameters of the B3LYP/6-31G* Optimized Structures of the Neutral *N*-L Ligands and Cu^+ $(N\text{-L})_x$ Complexes[a]

	bond length (Å)	bond angle (deg)		
species	Cu^+-N	∠NCCN	∠CCCC	∠NCu^+N
Cu^+(pyridine)	1.785			
Cu^+(pyridine)$_2$	1.835 (2)			180.0
Cu^+(pyridine)$_3$	1.933 (3)			120.0 (3)
Cu^+(pyridine)$_4$	2.016 (4)			111.6 (4)
				105.1 (2)
4,4-dipyridyl			36.2	
Cu^+(4,4-dipyridyl)	1.780		32.8	
Cu^+(4,4-dipyridyl)$_2$	1.832 (2)		33.9 (2)	179.9
Cu^+(4,4-dipyridyl)$_3$	1.930 (3)		34.5 (3)	120.0 (3)
Cu^+(4,4-dipyridyl)$_4$	2.018 (4)		34.3 (4)	111.8 (4)
				104.9 (2)
trans-2,2-dipyridyl		180.0	180.0	
cis-2,2-dipyridyl		35.1	35.4	
Cu^+(2,2-dipyridyl)	1.877 (2)	17.3	17.3	95.3
Cu^+(2,2-dipyridyl)$_2$	1.991 (4)	10.7 (2)	11.5 (2)	134.9 (2)
				114.5 (2)
				83.1 (2)
Cu^+(2,2-dipyridyl)$_3$	3.076 (2)	40.5 (2)	40.3 (2)	154.7 (2)
	2.036 (2)	18.4	19.8	144.8
	2.025 (2)			124.1
				117.7
				104.3
				97.6 (5)
				80.2 (2)
				64.5 (2)
1,10-phenanthroline		0.0		
Cu^+(1,10-phenanthroline)	1.881 (2)	0.0		96.2
Cu^+(1,10-phenanthroline)$_2$	2.000 (4)	0.0		123.5 (4)
				84.5 (2)
Cu^+(1,10-phenanthroline)$_3$	2.010 (2)	3.7		169.5 (2)
	2.135 (2)	3.7		123.7 (2)
	2.807 (2)	2.6		113.7 (2)
				108.0 (4)
				87.6 (2)
				79.3 (3)

[a] Average values are given in cases where more than a single bond distance or angles are similar, while degeneracies are given in parentheses.

bound to Cu^+ increases from one to four as a result of increasing ligand−ligand repulsion (Table 3).

Cu^+(2,2-Dipyridyl)$_x$. The complexation of 2,2-dipyridyl involves interaction of Cu^+ with the lone pair(s) of electrons of the nitrogen atom(s). In ground-state neutral 2,2-dipyridyl, the two pyridinyl rings are coplanar and the two nitrogen atoms are located on opposite sides of the central C−C bond, i.e., the trans-conformer of 2,2-dipyridyl shown in Figure 1. Complexation of 2,2-dipyridyl to Cu^+ can occur directly to this conformation, but much stronger binding is achieved when one of the pyridyl rings rotates to orient both N atoms so that they may simultaneously interact with the Cu^+ ion such that the ∠NCCN dihedral angle decreases from 180° to 17.3°, somewhat smaller than the 35.1° dihedral angle in the cis-conformer of neutral 2,2-dipyridyl. The ∠NCCN dihedral angle decreases further to 10.7° in the bis-complexes as a result of ligand−ligand repulsive interactions. In the bis-complexes the angle between the planes of the pyridyl rings of the two ligands is ∼60°. The ∠NCu^+N in the mono-ligated complex is 95.3°, decreases to 83.1° in the bis-complex, and to 64.5° in the tris-complex. The Cu^+(2,2-dipyridyl)$_3$ complex has a distorted octahedral structure with four similar, comparatively shorter, Cu^+-N bonds that lie nearly in a plane and two longer Cu^+-N bonds that lie above and below the plane. In this complex, two of the 2,2-dipyridyl ligands have ∠NCCN dihedral angles of 40.3°, while the third exhibits an angle of 18.4°. The Cu^+-N bond lengths in the Cu^+(2,2-dipyridyl)$_x$ complexes increase from 1.877 to 2.031 Å (3.076 Å for the two longer Cu^+-N bonds of the Cu^+(2,2-dipyridyl)$_3$ complex) as the number of 2,2-dipyridyl ligands bound to Cu^+ increases from one to three as a result of increasing ligand−ligand repulsion (Table 3).

Cu^+(1,10-Phenanthroline)$_x$. Neutral 1,10-phenanthroline has a planar π network with three cyclic components. Binding in the Cu^+(1,10-phenanthroline) complex is similar to that observed for Cu^+(2,2-dipyridyl) except that the Cu^+-N bonds lengths are slightly larger, 1.881 Å versus 1.877 Å. Because of the constrained ligand geometry of 1,10-phenanthroline, the ∠NCCN remains unchanged when it interacts with Cu^+. In the Cu^+(1,10-phenanthroline)$_2$ complex, the two 1,10-phenanthroline molecules bind to Cu^+ such that the π networks of the two ligands are perpendicular to each other to minimize repulsive interactions between the ligands. Similar to that observed for the Cu^+(2,2-dipyridyl)$_x$ complexes, the ∠NCu^+N angle decreases with increasing ligation, and varies from 96.2° to 84.0° to 79.3° for the mono-, bis-, and tris- complexes as a result of the longer Cu^+-N bond distances. The longer Cu^+-N bond distances observed in the Cu^+(1,10-phenanthroline)$_x$ complexes, as compared to the other *N*-L ligands, arise as a result of the highly constrained geometry of the ligand. The Cu^+(1,10-phenanthroline)$_3$ complex has a distorted octahedral structure with four comparatively shorter Cu^+-N bonds, that nearly lie in a plane and two longer Cu^+-N bonds, that lie above and below the plane. In this complex, the normally planar π network of the 1,10-phenanthroline ligands becomes slightly distorted due to the strong ligand−ligand repulsion. Two of the 1,10-phenanthroline ligands exhibit ∠NCCN dihedral angles of

TABLE 4: Second-Order Perturbation Energies *E*(2) (in kJ/mol) of Donor → Acceptor Interactions between Cu^+ and *N*-L Ligand(s) in Cu^+ (*N*-L)$_x$, Complexes at the B3LYP/6-311+G(2d,2p) Level of Theory[a]

donor → acceptor interaction	Cu^+(pyridine)	Cu^+(4,4-dipyridyl)	Cu^+(pyridine)$_2$	Cu^+(2,2-dipyridyl)	Cu^+(1,10-phenanthroline)
			Ligand-to-Metal σ Donation		
LP(N) → LP*(Cu)	215.2	219.7	351.0 (2)	144.6 (2)	145.9 (2)
LP(N) → RY*(Cu)	4.2	4.4	5.4	7.3 (2)	7.1 (2)
BD(N−C) → LP*(Cu)	9.3 (2)	9.5 (2)	17.7 (2)	11.5 (2), 6.8 (2)	11.8 (2), 7.3 (2)
CR(N) → LP*(Cu)	6.8	6.9	11.1	5.2 (2)	5.1 (2)
			Metal-to-Ligand π Backdonation		
LP(Cu) → RY*(N)	5.2	5.2	8.8	6.0 (2)	10.0 (2)
LP(Cu) → BD*(N−C)	12.2	17.2	6.2 (2)	6.3 (2), 5.2 (2)	6.9 (2), 6.4 (2)
CR(Cu) → BD*(N−C)	5.5 (2)	5.5 (2)	5.3 (2)	7.9 (2)	8.6 (2)
total NBO stabilization energy	273.2	283.4	785.7	401.6	418.2

[a] Only *E*(2) energies above 5.0 kJ/mol are shown. Orbital designations are defined as follows: BD = two-center bond, CR = one-center core pair, LP = one-center lone pair, RY* = one-center Rydberg orbitals, and BD* = two-center antibonding orbitals.

3.7°, while the third exhibits a dihedral angle of 2.6°. The Cu^+−N bond lengths in the Cu^+(1,10-phenanthroline)$_x$ complexes increase from 1.881 to 2.010 Å (2.807 Å for the two longer Cu^+−N bonds of the Cu^+(1,10-phenanthroline)$_3$ complex) as the number of 1,10-phenanthroline ligands bound to Cu^+ increases from one to three as a result of increasing ligand−ligand repulsion (Table 3).

Trends in the Cu^+−N bond lengths appear to be most closely linked to the flexibility of the ligand framework, rather than the relative bond strengths. The Cu^+(pyridine)$_x$ and Cu^+(4,4-dipyridyl)$_x$ complexes exhibit virtually identical Cu^+−N bond lengths that are shorter than those in the Cu^+(2,2-dipyridyl)$_x$ complexes, which in turn are shorter than those in the Cu^+(1,10-phenanthroline)$_x$ complexes. This parallels the flexibility of these ligands, and therefore, their ability to make structural changes to optimize the binding interactions. The more highly constrained geometry of the chelating ligands does not allow both N atoms to achieve an optimal binding orientation with Cu^+ and results in slightly longer Cu^+−N bond distances.

NBO Analyses. NBO analyses were performed for the Cu^+(pyridine), Cu^+(4,4-dipyridyl), Cu^+(pyridine)$_2$, Cu^+(2,2-dipyridyl), and Cu^+(1,10-phenanthroline) complexes. The corresponding stabilization energies were obtained between the electron donor−acceptor orbitals. Relevant orbital results are listed in Table 4. The most significant ligand-to-metal and metal-to-ligand donor−acceptor interactions of the Cu^+(pyridine)$_2$, Cu^+(2,2-dipyridyl), and Cu^+(1,10-phenanthroline) complexes are shown in Figure 8. The NBO analyses reveal that the dominant donor−acceptor interaction(s) in these complexes arise from σ donation of the lone pair of electrons of the pyridyl N atom, LP(N), to an antibonding orbital on Cu^+, LP*(Cu). As can be seen in the Figure 8, these interactions look remarkably similar for these three complexes. The total *E*(2) stabilization energies associated with the LP(N) → LP*(Cu) interactions are calculated to be 215.2, 219.7, 702.0, 289.2, and 291.8 kJ/mol for the Cu^+(pyridine), Cu^+(4,4-dipyridyl), Cu^+(pyridine)$_2$, Cu^+(2,2-dipyridyl), and Cu^+(1,10-phenanthroline) complexes, respectively. Given that the *E*(2) stabilization energy for the Cu^+(pyridine)$_2$ complex is more than twice as large as that computed for Cu^+(pyridine) suggests that the second pyridine molecule should be more strongly bound than the first. However, this contrasts both experimental and theoretical observations. The weaker binding of the second pyridine molecule is probably due to the very strong binding of the first pyridine ligand, which leaves less effective charge on Cu^+ and results in weaker binding of additional ligands. The stabilization energies for the complexes to the chelating ligands are somewhat larger than for a single pyridine or 4,4-dipyridyl ligand, but significantly lower than for interaction of Cu^+ with two pyridine ligands. This

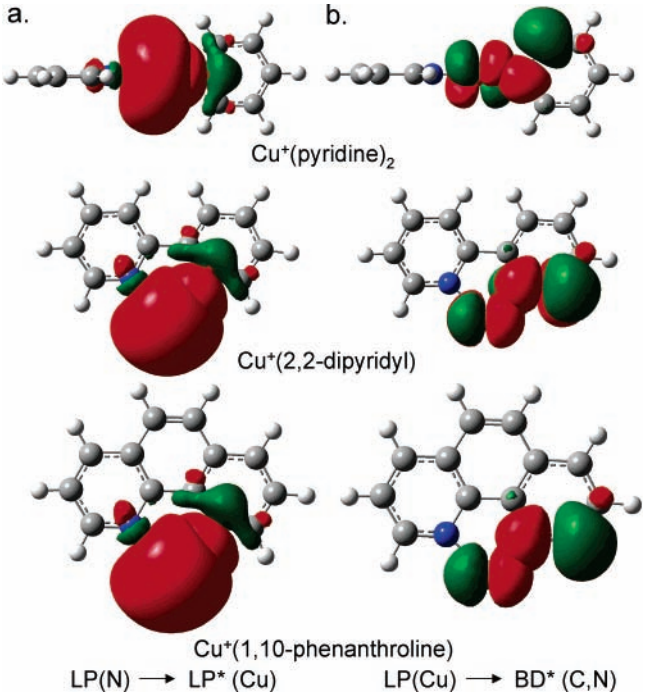

Figure 8. The most significant donor→acceptor orbital interactions of Cu^+(pyridine)$_2$, Cu^+(2,2- dipyridyl), and Cu^+ (1,10-phenanthroline). (a) Ligand-to-metal σ-donation LP(N) → LP*(Cu) and (b) metal−to−ligand π-backdonation LP(Cu) → BD*(CN). Only one of the two equivalent interactions for each is shown in the figure.

parallels the trends in the calculated and measured BDEs (i.e., the bidentate ligands bind more strongly than the mondentate ligands, but not as strongly as two independent monodentate ligands). In addition, the calculated *E*(2) stabilization for the Cu^+(pyridine)$_2$ complexes greatly exceeds the measured and calculated BDEs (Table 2), suggesting that the stabilization gained via this interaction is overestimated for this complex. Examination of the donor−acceptor contributions in the Cu^+(pyridine)$_2$ complex appear as though this overestimation may arise as a result of the symmetry of the complex such that the LP(N) → LP$^+$(Cu) is somehow double counted. If this is the case, and one of these contributions is discounted, then the total NBO stabilization energy reduces to 434.7 kJ/mol, in much better accord with the stabilization energies computed for the other complexes. Additional minor ligand-to-metal σ donation interactions, (LP(N) → RY*(Cu), BD(CN) → LP*(Cu), and BD(CN) → RY*(Cu)) also contribute to the binding in these complexes. Binding in these Cu^+(*N*-L)$_x$ complexes is also enhanced by metal-to-ligand π-backdonation interactions from both the valence d and core orbitals of Cu^+ to the antibonding

TABLE 5: Enthalpies and Free Energies of Binding of Ground State Cu^+ $(N\text{-L})_x$ Complexes at 0 and 298 K in kJ/mol[a]

complex	ΔH_0	ΔH_0[b]	$\Delta H_{298} - \Delta H_0$[b]	ΔH_{298}	ΔH[b]	$T\Delta S_{298}$[b]	ΔG_{298}	ΔG_{298}[b]
Cu^+(pyridine)	262.3 (7.7)	262. 0	1.7 (1.0)	264.0 (7.7)	263. 7	31.6 (4.1)	232.4 (8.7)	232.1
Cu^+(pyridine)$_2$	236.3 (8.7)	238. 9	−1.2 (0.9)	235.1 (8.7)	237. 7	46.4 (6.1)	188.7 (10.6)	191.3
Cu^+(pyridine)$_3$	82.4 (2.2)	48.8	−0.8 (0.6)	81.6 (2.3)	48.0	44.4 (7.4)	37.2 (7.7)	3.6
Cu^+(pyridine)$_4$	60.2 (2.6)	37.3	−4.1 (1.3)	56.1 (2.9)	33.2	50.4 (8.2)	5.7 (8.7)	−17.2
Cu^+(4,4-dipyridyl)	263.7 (10.6)	263. 1	1.3 (0.8)	265.0 (10.6)	264. 4	31.8 (4.2)	233.2 (11.4)	232.6
Cu^+(4,4-dipyridyl)$_2$	232.8 (7.0)	226. 4	−1.9 (0.2)	230.9 (7.0)	224. 5	46.7 (9.9)	184.2 (12.1)	177.8
Cu^+(4,4-dipyridyl)$_3$	63.4 (1.6)	34.9	−1.1 (2.1)	62.3 (2.6)	33.8	46.8 (6.8)	15.5 (7.3)	−13.0
Cu^+(4,4-dipyridyl)$_4$		32.8	−2.4 (2.3)		30.4	49.6 (8.1)		−19.2
Cu^+(2,2-dipyridyl)	370.3 (12.9)	358. 9	2.0 (0.4)	372.3 (12.9)	360. 9	35.1 (2.6)	337.2 (13.1)	325.8
Cu^+(2,2-dipyridyl)$_2$	237.7 (9.7)	227. 0	−1.2 (0.3)	236.5 (9.7)	225. 8	53.5 (8.4)	183.0 (12.8)	172.3
Cu^+(2,2-dipyridyl)$_3$		−46. 9	−18.9 (1.2)		−65. 8	39.8 (4.7)		−105. 6
Cu^+(1,10-phenanthroline)	395.0 (12.5)	393. 2	2.0 (1.0)	397.0 (12.5)	395. 2	35.5 (5.2)	361.5 (13.5)	359.7
Cu^+(1,10-phenanthroline)$_2$	233.0 (4.1)	229. 2	−1.3 (0.9)	231.7 (4.2)	227. 9	53.1 (6.9)	178.6 (8.0)	174.8
Cu^+(1,10-phenanthroline)$_3$		−3.7	−4.1 (0.8)		−7.8	48.9 (8.2)		−56.7

[a] Uncertainties are listed in parentheses. [b] Density functional theory values from calculations at the B3LYP/6-311+G(2d,2p) level of theory using B3LYP/6-31G* optimized geometries with frequencies scaled by 0.9804.

orbitals of the pyridyl moieties, LP(Cu) → RY*(N), LP(Cu) → BD*(N−C), and CR(Cu) → BD*(N−C). These analyses indicate that metal-to-ligand π-backdonation is less significant for the monodentate ligands than the chelating ligands examined here. The stabilization gained via π-backdonation from Cu^+ to the monodentate ligands accounts for 10.4, 11.8, and 4.4% of the calculated stabilization for the Cu^+(pyridine), Cu^+(4,4-dipyridyl), and Cu^+(pyridine)$_2$ complexes, respectively. The π-backdonation from Cu^+ to the chelating ligands is somewhat enhanced to that found for the monodentate ligands, and accounts for 12.6 and 15.3% of the calculated stabilization for the Cu^+(2,2dipyridyl) and Cu^+(1,10-phenanthroline) complexes, respectively. The more favorable π-backdonation from Cu^+ to 1,10-phenanthroline, as compared to 2,2-dipyridyl or 2-pyridine ligands, arises because the filled d orbitals of Cu^+ overlap better with the π^* orbitals of the planar π network of 1,10-phenanthroline. Evidence for this can be seen in Figure 8, where the dominant donor−acceptor interactions for the Cu^+(pyridine)$_2$, Cu^+(2,2-dipyridiyl), and Cu^+(1,10-phenanthroline) complexes are shown. The Cu^+(1,10-phenanthroline) complex exhibits stronger π-backdonation because the orbitals involved lie in the same plane as the complex, whereas in the Cu^+(2,2-dipyridyl) complex, these orbitals are not as well aligned with those of the ligands as a result of the twist in the pyridyl rings to maximize bonding while minimizing ligand−ligand repulsion. Metal-to-Ligand π-backdonation is not as extensive for the Cu^+(pyridine)$_2$ complex because the orbitals of the pyridine ligand are not as extensive or as well matched energetically. Thus, the π acceptor ability of these ligands and the covalent character of the binding interactions should follow the order pyridine <4,4-dipyridyl, < 2,2-dipyridyl < 1,10-phenanthroline.

The NBO analyses also provide valuable information about the sd-hybridization in these complexes. For example, the ground-state electron configuration of isolated Cu^+ is $4s^0 3d^{10}$. The natural electron configurations of Cu^+ in the Cu^+(pyridine) and Cu^+(4,4-dipyridyl)are identical and are $4s^{0.28}$ $3d^{9.86}$, while the Cu^+(pyridine)$_2$ complex exhibits a configuration of $4s^{0.52}$ $3d^{9.76}$ $4p^{0.01}$. These results clearly show that the 4s and 3d orbitals are hybridized to help minimize Pauli repulsion between Cu^+ and the ligand(s), but that the extent of hybridization increases upon binding of the second ligand. The increased occupation of the s orbital in the Cu^+(pyridine)$_2$ complex leads to greater Pauli repulsion between Cu^+ and the pyridine ligand-(s), explaining why the second pyridine ligand binds less strongly than the first. The natural electron configurations of Cu^+ in the Cu^+(1,10-phenanthroline), and Cu^+(2,2-dipyridyl) complexes are identical and are $4s^{0.23}$ $3d^{9.87}4d^{0.01}5d^{0.01}$. Clearly, sd-hybridization also occurs for these complexes, but to an extent similar to that found for binding of a single monodentate ligand.

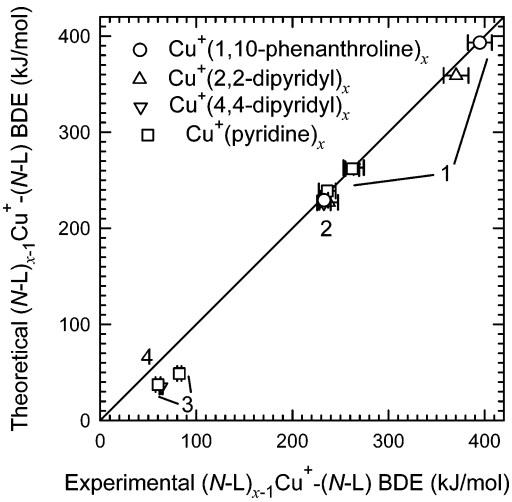

Figure 9. Theoretical vs experimental $(N\text{-L})_{x-1}Cu^+-(N\text{-L})_x$ BDEs at 0 K (in kJ/mol), where *N*-L include 1,10-phenanthroline (○), 2,2-dipyridyl (△), 4,4-dipyridyl (▽), and pyridine (□). The diagonal line indicates the values for which calculated and measured BDEs are equal.

Conversion from 0 to 298 K. The 0 K BDEs determined here (experimentally and theoretically) are converted to 298 K bond enthalpies and free energies. The enthalpy and entropy conversions are calculated using standard formulas (assuming harmonic oscillator and rigid rotor models) and the vibrational and rotational constants determined for the B3LYP/6-31G* optimized geometries. Table 5 lists 0 and 298 K enthalpy, free energy, and enthalpic and entropic corrections for all systems studied. Uncertainties in the enthalpic and entropic corrections are determined by 10% variation in the molecular constants. Because theory may not adequately describe the weak interactions in these systems, the listed uncertainties also include contributions from scaling all frequencies below 150 cm^{-1} up and down by a factor of 2.

Discussion

Comparison of Theory and Experiment. The BDEs for the Cu^+ $(N\text{-L})_x$ complexes, where *N*-L = pyridine ($x = 1-4$), 4,4-dipyridyl ($x = 1-3$), 2,2-dipyridyl ($x = 1-2$), and 1,10-phenanthroline ($x = 1-2$) at 0 K, measured here by guided ion

beam mass spectrometry are summarized in Table 2. The BDEs listed for the $x = 3$ and 4 complexes are those obtained from fits to the total cross sections. Also listed in Table 2 are the 0 K BDEs calculated at the B3LYP/6-311+G(2d,2p)//B3LYP/6-31G* level of theory, including ZPE and BSSE corrections. The agreement between the calculated and measured BDEs for all of the Cu^+ (*N*-L)$_x$ complexes is illustrated in Figure 9. As can be seen in the figure, the agreement between experiment and theory is excellent for all systems except the Cu^+(pyridine)$_3$, Cu^+(pyridine)$_4$, and Cu^+(4,4-dipyridyl)$_3$ complexes, where the theoretical values are systematically low.

We had previously measured the BDE of the Cu^+(pyridine) complex,[60] while the present results are the first measurements of the BDEs of Cu^+(pyridine)$_x$, $x = 2-4$. As can be seen in Figure 9, excellent agreement between theory and experiment is found for the $x = 1$ and 2 complexes. However, the theoretical BDEs of the Cu^+(pyridine)$_3$ and Cu^+(pyridine)$_4$ complexes are lower than the experimentally determined values by 33.6 and 22.9 kJ/mol, respectively. This difference is much larger than the experimental error in these measurements, 2.2 and 2.6 kJ/mol, respectively. The mean absolute deviation (MAD) between the experimentally measured and calculated values for all four Cu^+(pyridine)$_x$ complexes is 14.8 ± 16.1 kJ/mol. When the Cu^+(pyridine)$_3$ and Cu^+(pyridine)$_4$ complexes are not included the MAD is very low, 1.5 ± 1.6 kJ/mol. The largest discrepancy between the theoretical and the experimental BDEs is observed for the Cu^+(pyridine)$_3$ complex, as was also found for the Cu^+(imidazole)$_x$ systems we previously examined.[65] It is unclear why the agreement between theory and experiment is less satisfactory when Cu^+ binds with more than two ligands. The Gibbs free energy at 298 K for the loss of pyridine from the Cu^+(pyridine)$_4$ complex is calculated to be a spontaneous reaction and, therefore, suggests that is not bound at room temperature. However, our ability to observe Cu^+(pyridine)$_4$ and measure its CID behavior clearly establish that this species is bound and loss of a single pyridine ligand from this complex is endoergic. Furthermore, the calculated Gibbs free energy for loss of pyridine from Cu^+(pyridine)$_3$ is relatively small and much smaller than the average internal energy of the complex at 298 K. Therefore, this complex would also dissociate at room temperature. Again, our ability to produce Cu^+(pyridine)$_3$ in large abundance and measure its CID behavior again indicates that loss of pyridine from this complex is endoergic. This evidence suggests that theory systematically underestimates the BDEs of the Cu^+(pyridine)$_3$ and Cu^+(pyridine)$_4$ complexes.

The BDEs of Cu^+(4,4-dipyridyl)$_x$, where $x = 1-3$, show similar behavior to that observed for the Cu^+(pyridine)$_x$ complexes. Excellent agreement between theory and experiment is observed for Cu^+ binding to one or two 4,4-dipyridyl ligands, whereas less satisfactory agreement is found for the Cu^+(4,4-dipyridyl)$_3$ system. As for Cu^+(pyridine)$_4$, theoretical calculations suggest that loss of 4,4-dipyridyl from Cu^+(4,4-dipyridyl)$_3$ would be a spontaneous reaction. This is clearly not the case because again the experimental observation of this complex and the observed CID behavior suggest that this reaction is endoergic. Therefore, the poor agreement can again be attributed to limitations of the level of theory used to describe these interactions. The MAD for all three Cu^+(4,4-dipyridyl)$_x$ systems is 10.3 ± 12.1 kJ/mol, larger than the average experimental uncertainty (AEU) in these measurements, 6.4 ± 4.5 kJ/mol. When the Cu^+(4,4-dipyridyl)$_3$ complex is not included the MAD decreases to 3.5 ± 4.1 kJ/mol. We were unable to make an appreciable ion beam of the Cu^+(4,4-dipyridyl)$_4$ complex because its average internal energy at room temperature exceeds the calculated BDE, and therefore could not measure its CID behavior.

We have determined the BDEs of Cu^+(2,2-dipyridyl)$_x$ complexes, where $x = 1$ and 2. Excellent agreement between theory and experiment is found. The MAD for the two Cu^+(2,2-dipyridyl)$_x$ complexes is 11.0 ± 0.5 kJ/mol, similar to the AEU in these measurements of 11.3 ± 2.3 kJ/mol. Likewise, excellent agreement between theory and experiment is observed for the Cu^+(1,10-phenanthroline)$_x$ complexes, where $x = 1$ and 2. The MAD for the Cu^+(1,10-phenanthroline)$_x$ complexes is 2.8 ± 1.4 kJ/mol, smaller than the AEU in these measurements, 8.3 ± 5.9 kJ/mol. We were also unable to make appreciable ion beams of the Cu^+(2,2-dipyridyl)$_3$ and Cu^+(1,10-phenanthroline)$_3$ complexes because their average internal energies at room temperature exceed the calculated BDEs. In fact, theory predicts that neither of these species are bound relative to the corresponding isolated bis-complex and neutral ligand even though a stable structure is calculated for both systems.

Comparison with Literature Values. Table 2 compares the present experimental results for the BDE of the Cu^+(pyridine) complex to that previously measured in our laboratory using the same threshold collision-induced dissociation (TCID) techniques as employed here,[60] and that determined by Yang et al. using photodissociation techniques.[66] The BDE for the Cu^+(pyridine) complex measured here is 16.4 kJ/mol larger than the value previously determined by TCID, but is still within the combined uncertainties in these measurements. In the previous study, evidence for a small population of excited-state species in the reactant ion beam was observed as a small low-energy feature in the Cu^+ product cross section. When present, such features complicate the threshold analysis, making it more difficult to extract an accurate value and generally provide values that are too low. Therefore, the value determined here is expected to be more reliable. The experimental value measured by Yang et al., 274.1 ± 75.2 kJ/mol, is 11.8 kJ/mol larger than the BDE measured here. This difference is larger than the uncertainty in our value, but well within the large uncertainty in their measurement. In addition, the BDE of Cu^+(pyridine) measured here (262.3 ± 7.7 kJ/mol) is in excellent agreement with the calculated value (262.0 kJ/mol). This suggests that the BDE of the Cu^+(pyridine) complex determined here provides the most accurate value determined for the binding in this complex.

Complexing Ability of the *N*-L Ligands. The ground-state structures of the neutral *N*-L ligands are shown in Figure 1 along with their calculated dipole moments and isotropic molecular polarizabilities. The ground-state structures of the Cu^+(*N*-L)$_x$ complexes are shown in Figures 4 through 7. In each of these complexes Cu^+ interacts with one to six N atoms. The variation in the number of N donor atoms interacting with Cu^+, and the differences in the dipole moments, polarizabilities, and flexibility of these ligands, produces both geometrical and energetic differences in the binding.

Pyridine is able to achieve a nearly ideal arrangement of the N atoms around Cu^+ so as to minimize ligand−ligand repulsive interactions. Similarly, 4,4-dipyridyl is also able to achieve nearly ideal geometry in its binding interactions to Cu^+. Ligands such as 2,2-dipyridyl and 1,10-phenanthroline with two or more donor centers are suitable to coordinate with metal cations and incorporate the ion into a ring, in both cases a relatively stable five-membered ring. Although the metal complexes of 4,4-dipyridyl possess the same number of analogous donor

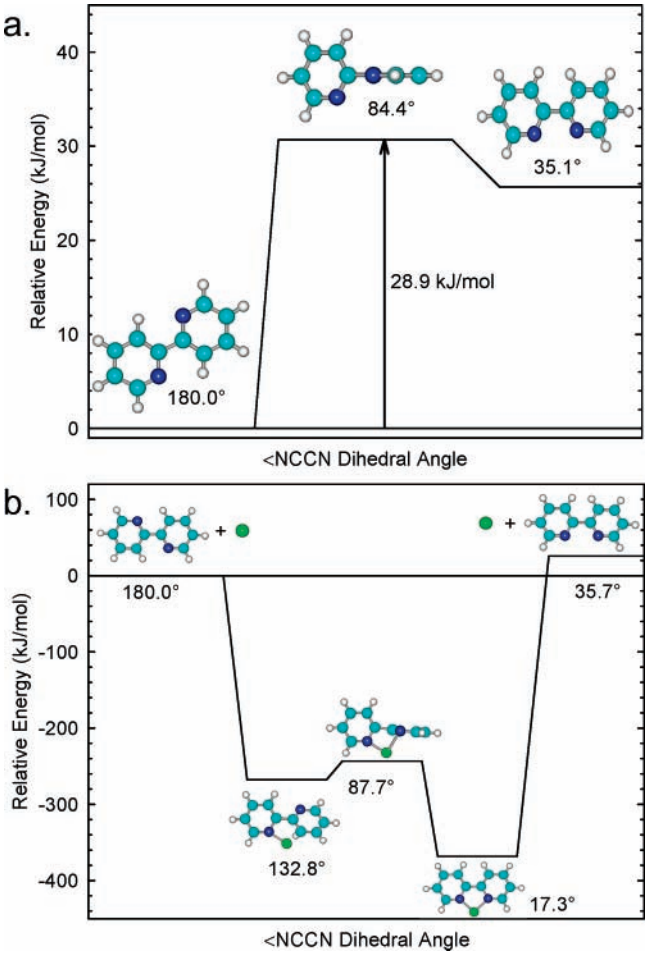

Figure 10. Potential energy landscapes at 0 K for (a) unimolecular interconversion of cis- and trans-2,2-dipyridyl and (b) association of Cu^+ and 2,2-dipyridyl and interconversion of the cis- and trans-bound Cu^+(2,2-dipyridyl) complexes. Energies determined from calculations at the B3LYP/6-311+G(2d,2p) level of theory including ZPE and BSSE corrections.

centers their complexing ability differs considerably because they are geometrically constrained such that only one N atom may bind to a given metal center.

The complexation of 2,2-dipyridyl by Cu^+ forces the two N atoms to orient themselves to interact with Cu^+. Figure 10 shows the potential energy landscape for the conversion of *trans*- and *cis*-2,2-dipyridyl. The energy barrier for this transition at 0 K is calculated to be 28.9 kJ/mol. The potential energy landscape for the conversion of monodentate Cu^+(trans-2,2-dipyridyl) into the bidentate Cu^+(cis-2,2-dipyridyl) complex is also shown in Figure 10. The energy barrier calculated for this transition at 0 K is 24.6 kJ/mol. Thus interaction with Cu^+ slightly facilitates this conversion. Upon complexation to Cu^+, 2,2-dipyridyl becomes more constrained, but rotation about the central C−C bond is still possible such that the pyridyl rings twist to minimize ligand−ligand repulsion while maximizing binding to Cu^+. The aromatic system of 1,10-phenanthroline constrains this ligand to a planar geometry such that these ligands orient themselves perpendicular to each other to minimize ligand−ligand repulsive interactions in the bis-complexes. Ligand−ligand repulsion becomes significant enough in the Cu^+(1,10-phenanthroline)$_3$ complex that the ligands distort slightly from planarity.

All of these *N*-L ligands are strong σ donors and weak π acceptors. The lone pairs of electrons on the N atoms donate electron density to a hybridized 4s3d orbital of the Cu^+ ion. Using the aromatic systems of these *N*-L ligands, the occupied

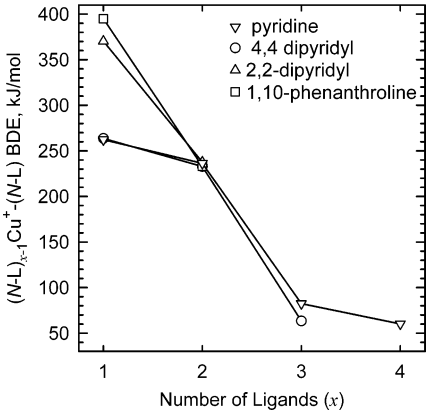

Figure 11. Experimental [$(N\text{-L})_{x-1}Cu^+$−*N*-L] BDEs at 0 K (in kJ/mol) as a function of the number of *N*-L ligands, *x*.

orbitals of Cu^+, having the appropriate geometry, can overlap with the unoccupied π^* orbitals of the ligands. Both binding interactions act synergistically to produce very strong binding to Cu^+ that is primarily noncovalent in nature.

As strong σ donors, the ability of these *N*-L ligands to complex Cu^+ is largely determined by their dipole moments and polarizabilities. Although 4,4-dipyridyl exhibits no net dipole moment, the local dipole moments of the pyridyl rings should be virtually identical to that of pyridine, 2.31 D. This coupled with the very small differences in the Cu^+−N bond lengths and similarities in the binding interactions should lead to ion-dipole interactions in the Cu^+(pyridine)$_x$ and Cu^+(4,4-dipyridyl)$_x$ complexes of equivalent strength. The dipole moments of 2,2-dipyridyl and 1,10-phenanthroline are 3.04 and 3.31 D, respectively. Thus the ion−dipole interactions to these chelating ligands should be ~32% and 43% stronger than to pyridine and 4,4-dipyridyl. The calculated molecular polarizabilities of pyridine, 4,4-dipyridyl, *cis*-2,2-dipyridyl, and 1,10-phenanthroline are 9.27, 19.32, 19.67, and 23.78 Å^3, respectively. Thus, the ion-induced dipole interactions should be the weakest for the Cu^+(pyridine)$_x$ complexes, similar and slightly more than twice as strong for the Cu^+(4,4-dipyridyl)$_x$ and Cu^+(2,2-dipyridyl)$_x$ complexes, and largest (more than 2.5 times as large) for the Cu^+(1,10-phenanthroline)$_x$ complexes. The magnitude of the ligand−ligand repulsive interactions should also parallel the ion-induced dipole interactions as a result of both the relative sizes and flexibilities of these *N*-L ligands. However, for complexes with the same number of Cu^+−N interactions, those complexes to pyridine and 4,4-dipyridyl will possess twice as many ligands as those to 2,2-dipyridyl and 1,10-phenanthroline, and thus the ligand−ligand repulsive interactions would be expected to be smaller for the complexes to the chelating ligands. Finally, the binding in these complexes is enhanced by metal-to-ligand π-backdonation. Based upon the results of the NBO analyses performed here, the π acceptor abilities of these ligands follow the order pyridine < 4,4-dipyridyl < 2,2-dipyridyl < 1,10-phenanthroline. Therefore, the enhancement in the binding arising from metal-to-ligand π-backdonation and the degree of covalent character in the binding should also follow this order. Thus, the relative BDEs for the monoligated Cu^+(*N*-L) complexes are expected to follow the order Cu^+(pyridine) ≈ Cu^+(4,4-dipyridyl) < Cu^+(2,2-dipyridyl) < Cu^+(1,10-phenanthroline).

Trends in the Sequential Bond Dissociation Energies. As can be seen in Figure 11, the trends in the sequential BDEs of pyridine and 4,4-dipyridyl are remarkably similar. The BDEs for binding of the first and second ligand are quite strong, but

decrease somewhat from the first to the second ligand. A sharp decrease in the BDEs occurs for binding of the third ligand, whereas a fairly small decrease in the BDEs is observed from the third to the fourth ligand.

Similar behavior has been observed for the solvation of Cu^+ by several other ligands, e.g., water,[43] acetone,[67] acetonitrile,[68] ammonia,[69] dimethylether,[70] and imidazole.[65] The trends in the sequential binding energies of all of the $Cu^+(ligand)_x$ complexes are similar, except that the $Cu^+(imidazole)_2$, $Cu^+(acetonitrile)_2$, $Cu^+(pyridine)_2$, and $Cu^+(4,4\text{-dipyridyl})_2$ are somewhat weaker than their monoligated complexes, whereas the other ligands exhibit the opposite relative behavior for binding of the first and second ligands. This difference may arise because imidazole, acetonitrile, pyridine, and 4,4-dipyridyl are strong field ligands and therefore bind more strongly to Cu^+ than the other ligands. The binding of the second ligand is then weaker because its electron density overlaps with that of the first ligand to a greater extent. Moreover, the *N*-donor ligands bind more strongly to Cu^+ than *O*-donor ligands. This is not surprising because the N lone pairs are more basic than those of an O atom.

The trends in the sequential BDEs can be understood in terms of a balance of several competing factors, the electrostatic ion-dipole and ion-induced dipole attractions, sd-hybridization of Cu^+, and ligand−ligand repulsion.[71−73] The electrostatic contributions to the binding decrease upon sequential ligation because the effective charge retained by Cu^+ decreases and the Cu^+−N (or Cu^+−O) bond distances increase. Similarly, the repulsion between ligands increases upon sequential ligation, leading to weaker binding. If no other effects were operative the sequential BDEs would decrease monotonically, which is clearly not the case. The first and second BDEs are very strong compared to the third and fourth BDEs. This behavior is largely the result of sd-hybridization of Cu^+. The electronic configuration of Cu^+ is $4s^03d^{10}$, and therefore, the dσ orbital is occupied. Occupation of the dσ orbital leads to greater Pauli repulsion between the metal ion and the ligand than when it is unoccupied. 4s-3dσ hybridization effectively removes electron density from the metal−ligand axis by placing the electron density in a hybridized orbital that is perpendicular to the bonding axis. This allows the ligands to approach Cu^+ with minimum Pauli repulsion. The BDE of the second ligand is nearly as strong as the first ligand, but slightly weaker. The weaker binding in the bis-complexes is likely the result of two effects, the decline in the effective positive charge retained by Cu^+ upon binding to the first ligand, and the repulsive interactions between the electron density of the first and second ligands.

The effects of sd-hybridization lead to much weaker binding of additional ligands beyond the first two. If the stabilization gained via sd-hybridization is maximally diminished when the third ligand binds directly to Cu^+, a trigonal planar arrangement of the nitrogen atoms of the ligands with $\angle NCu^+N$ bond angles of 120° is expected in $Cu^+(pyridine)_3$ and $Cu^+(4,4\text{-dipyridyl})_3$. In contrast, the calculations find a slightly distorted trigonal planar structure for both of these complexes, suggesting that a minor amount of the stabilization gained by sd-hybridization is retained. Our calculations find that the $Cu^+(pyridine)_4$ and $Cu^+(4,4\text{-dipyridyl})_4$ complexes exhibit geometries with a nearly tetrahedral arrangement of the N atoms around Cu^+ suggesting that ligation by four ligands is enough to eliminate the stabilization associated with sd-hybridization.

The trends in the sequential BDEs of 2,2-dipyridyl and 1,10-phenanthroline are also remarkably similar, but differ from that observed for the monodentate ligands, pyridine and 4,4-dipyridyl. The BDEs for binding of the first ligand are very strong, and decrease sharply from the first to the second ligand, but are still quite strong. Indeed, the BDEs for the $Cu^+(N\text{-L})$ complexes increase by more than 100 kJ/mol on going from the monodentate to the chelating ligands. In contrast, the BDEs for loss of a single ligand from the $Cu^+(N\text{-L})_2$ complexes differ by less than 5 kJ/mol for all four of these *N*-L ligands. The more rapid decrease in the sequential BDEs for the complexes to 2,2-dipyridyl and 1,10-phenanthroline arise because the electrostatic contributions to the binding decrease more rapidly upon sequential ligation because the chelating ligands provide two donor interactions such that the charge retained by Cu^+ decreases more rapidly than for the complexes to the monodentate ligands. The ligand−ligand repulsive interactions are also larger for these larger chelating ligands.

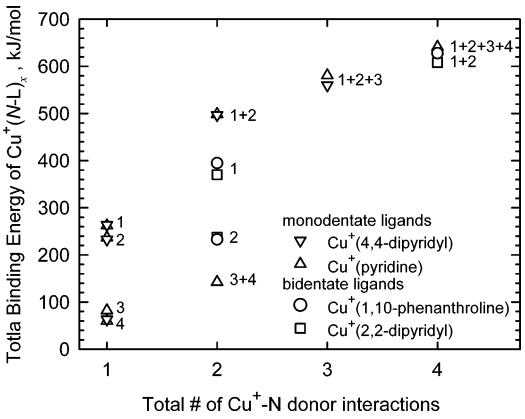

Figure 12. Trends in the total BDEs of $Cu^+(N\text{-L})_x$ complexes at 0 K (in kJ/mol) as a function of the number of *N*−donor interactions. Energies determined from calculations at B3LYP/6−311+G(2d,2p) level of theory including ZPE and BSSE corrections.

Although the chelating ligands, 1,10-phenanthroline and 2,2-dipyridyl, interact with Cu^+ via the lone pair of electrons on both N atoms, this binding is not as strong as the binding of two individual pyridine or 4,4-dipyridyl ligands. The constrained geometries of these chelating ligands do not allow optimum orientation of the two N atoms, and therefore these complexes are unable to take full advantage of sd-hybridization. For example, when Cu^+ binds to two ligands of pyridine or 4,4-dipyridyl, the $\angle NCu^+N$ bond angles are 180°, orienting the ligands as far apart from each other as possible, maximizing stabilization via sd-hybridization, and minimizing ligand−ligand repulsive interactions. When Cu^+ binds to 1,10-phenanthroline or 2,2-dipyridyl the $\angle NCu^+N$ bond angles are 90° and 82°, respectively. This constrained binding geometry leads to less stabilization via sd-hybridization resulting in less favorable binding than for two independent monodentate ligands.

Trends in the Total Bond Dissociation Energies. The total binding energies of the $Cu^+(N\text{-L})_x$ complexes are summarized in Table 2, while the trends in the total BDEs of these complexes as a function of the number of *N*-donor atoms interacting with Cu^+ are shown in Figure 12. The first 4,4-dipyridyl ligand binds slightly more strongly than pyridine as a result of its greater polarizability. However, the sequential BDEs to 4,4-dipyridyl decrease slightly more rapidly than those to pyridine because ligand−ligand repulsive interactions of the larger 4,4-dipyridyl ligands overcome the effects of the enhanced polarizability.

The sum of the binding energies for the first two ligands of $Cu^+(pyridine)_x$ and $Cu^+(4,4\text{-dipyridyl})_x$ are essentially equal because the binding interactions are very similar and are dominated by sd-hybridization of Cu^+. The enhanced binding arising from the increased polarizability of 4,4-dipyridyl is essentially cancelled by the increased ligand−ligand repulsive

interactions in the bis-complex. Chelating ligands with two *N*-donor atoms, 2,2-dipyridyl and 1,10-phenanthroline, exhibit weaker binding interactions to Cu^+ than the sum of the first two BDEs to pyridine and 4,4-dipyridyl. The weaker binding in the former complexes arises because the constrained geometry of these ligands does not allow them to take full advantage of the stabilization gained by sd-hybridization in the latter. As can be seen in Figure 12, 1,10-phenanthroline binds slightly more strongly to Cu^+ than 2,2-dipyridyl. This suggests that the larger dipole moment, polarizability, and better π-acceptor ability of 1,10-phenanthroline enhance the binding interaction more than the flexibility of 2,2-dipyridyl ligand. Binding of the second 2,2-dipyridyl or 1,10-phenanthroline ligands to Cu^+ is stronger than the sum of the third and fourth BDEs to pyridine. This suggests that these chelating ligands experience less ligand−ligand repulsion (two bidentate vs four monodentate ligands) as a result of their constrained ligand geometries. The sum of the binding energies for the first three pyridine molecules is slightly greater than that of 4,4-dipyridyl, again the result of the increased ligand−ligand repulsion in the larger 4,4-dipyridyl complexes.

The total energy required to completely dissociate $Cu^+(pyridine)_4$ into bare Cu^+ and four neutral pyridine ligands is slightly greater than that required to completely dissociate $Cu^+(1,10\text{-phenanthroline})_2$ and $Cu^+(2,2\text{-dipyridyl})_2$. In all of these complexes, Cu^+ interacts with four nitrogen donors. This suggests that the constrained geometry of these chelating ligands weakens the binding more than it reduces ligand−ligand repulsive interactions. However, the differences in the enthalpic contributions to the binding in these complexes are rather small compared to the total binding energy. Under equilibrium conditions or in solution, entropic effects will easily overcome the small differences in the total BDEs such that the free energies of binding will greatly favor the chelating ligands, 2,2-dipyridyl and 1,10-phenanthroline, over the monodentate ligands, pyridine and 4,4-dipyridyl.

Conclusions

The kinetic energy dependences of the collision-induced dissociation of 11 $Cu^+(N\text{-L})_x$ complexes, where *N*-L = pyridine ($x = 1-4$), 4, 4-dipyridyl ($x = 1-3$), 2,2−dipyridyl ($x = 1-2$), and 1,10-phenanthroline ($x = 1-2$), with Xe are examined in a guided ion beam tandem mass spectrometer. The dominant dissociation process observed for all of the complexes is loss of a single intact neutral *N*-L ligand. BDEs at 0 K are determined from the thresholds for these processes for all of the $Cu^+(N\text{-L})_x$ complexes. Structures, theoretical estimates for the measured BDEs, and insight into the nature of the binding of the $Cu^+(N\text{-L})_x$ complexes is provided by density functional theory calculations performed at the B3LYP/6-311+G(2d,2p)//B3LYP/6-31G* level of theory. Excellent agreement between theory and experiment is observed for all of the $Cu^+(N\text{-L})_x$ complexes, where $x = 1$ and 2. However, for the $x = 3$ and 4 complexes, theory systematically underestimates the strength of the binding.

The chelating ligands, 2,2-dipyridyl and 1,10-phenanthroline, exhibit very strong binding as compared to a single monodentate ligand, pyridine or 4,4-dipyridyl. The binding to these chelating ligands involves interaction with two N donor atoms, but is weaker than the sum of two independent pyridine or 4,4-dipyridyl ligands, a consequence of geometric restrictions that do not allow optimal orientation of the donor atoms around the Cu^+ ion. However, the enthalpic contributions to the binding for all of the $Cu^+(N\text{-L})_x$ complexes involving four N donor interactions are nearly equal. Thus, the larger formation constants for the binding in the $Cu^+(N\text{-L})_x$ complexes to the chelating ligands in solution are almost entirely the result of entropic contributions to the binding.

Acknowledgment. This work is supported by the National Science Foundation, Grant CHE-0518262.

Supporting Information Available: Tables of vibrational frequencies, average vibrational energies at 298 K, and rotational constants of the neutral *N*-L ligands and $Cu^+(N\text{-L})_x$ complexes in their ground state conformations. Figures showing cross sections for CID of $Cu^+(N\text{-L})_x$ with Xe as well as empirical fits to the primary product channels. This material is available free of charge via the Internet at http:/pubs.acs.org.

References and Notes

(1) Lehninger, A. L. *Biochemistry*, 3rd ed.; Worth Publishers: New York, 1996.
(2) Brody, F.; Ruby, P. R. In *Heterocyclic Compounds, Pyridine and Derivatives*; Klingsberg, E., Ed.; Interscience Publishers: New York, 1960; Part I.
(3) Veal, J. M.; Rill, R. L. *Biochemistry* **1989**, *28*, 3243.
(4) Sigman, D. S.; Bruice, T. W.; Mazumder, A.; Sutton, C. L. *Acc. Chem. Res.* **1993**, *26*, 98.
(5) Anipsitakis, G. P.; Dionysiou, D. D. *Appl. Catal., B* **2004**, *54*, 155.
(6) Tung, K.; Presley, B. J. *Anal. Chem.* **2002**, *74*, 4716.
(7) Xu, G.; Dong, S. *Anal. Chem.* **2000**, *72*, 5308.
(8) Saravanabharathi, D.; Samuelson, A. G. *Indian J. Chem.* **2003**, *42A*, 2300.
(9) Vogtle, F. *Supramolecular Chemistry*, 2nd ed.; John Wiley & Sons: New York, 1991.
(10) Norkus, E.; Stalnioniene, I.; Crans, C. D. *Heteroat. Chem.* **2003**, *7*, 625.
(11) Sigman, S. D.; Bruice, T. W.; Mazumder, A.; Sutton, C. L. *Acc. Chem. Res.* **1993**, *26*, 98.
(12) Papavassiliou, A. G. *Biochem. J.* **1995**, *305*, 345.
(13) Sigman, S. D.; Graham, D. R.; Stern, A. M. *J. Biol. Chem.* **1979**, *254*, 12262.
(14) Sigman, S. D *Acc. Chem. Res.* **1986**, *19*, 180.
(15) Thimann, K. V.; Satler, S. *Proc. Natl. Acad. Sci. U.S.A.* **1979**, *76*, 2770.
(16) Earl, J. W.; Kennedy, R. K. *Phytochemistry* **1975**, *14*, 1907.
(17) Richardson, J. N.; Dyer, L. D. *Anal. Chem.* **2002**, *74*, 3330.
(18) Gao, L.; Seliskar, C. J.; Heinman, W. K. *Anal. Chem.* **1999**, *71*, 4061.
(19) JongMan, K.; Byongoh, C.; KiHong, P.; Tae-Eun, C.; DongKeun, H. *Polymer Bull. (Berlin)* **2000**, *44*, 79.
(20) Arena, G.; Contino, A.; Longo, E.; Zito, V. *Chem. Commun.* **2004**, *16*, 1812.
(21) Li, J.; Hayden, H.; Kohl, P. *Electrochim. Acta* **2004**, *49*, 1789.
(22) Oscafrain, M.; Devaud, M.; Perichon, J. *Electrochim. Acta* **1997**, *42*, 99.
(23) Hou, K. Y.; Yu, L.; Serverson, M.; Zeng, Z. *J. Phys. Chem. B* **2005**, *109*, 9527.
(24) Ananraj, J.; Srinivasan, S.; Ponvel, K.; Athappan, P. *J. Inorg. Biochem.* **2005**, *99*, 669.
(25) Yang, D.; Bizzotto, D.; Lipkowski, J.; Pettinger, B.; Mirwald. S. *J. Phys. Chem.* **1994**, *98*, 7083.
(26) Zhang, C.; Haruyama, T.; Kobatake, E.; Aizawa, M. *Anal. Chim. Acta* **2000**, *408*, 225.
(27) Piguet, C.; Bernardinelli, G.; Hopfgartner, G. *Chem. Rev.* **1997**, *97*, 2005.
(28) Knof, U.; von Zelewsky, A. *Angew. Chem., Int. Ed. Engl.* **1999**, *38*, 303.
(29) Belser, P.; Bernhard, S.; Jandrasics, E.; von Zelewsky, A.; De, Cola, L.; Balzani, V. *Coord. Chem. Rev.* **1997**, *159*, 11.
(30) Kalyanasundaram, K.; Grätzel, M. *Coord. Chem. Rev.* **1998**, *177*, 347.
(31) Baxter, S. M.; Jones, Jr., W. E.; Danielson, E.; Worl, L.; Strouse, G.; Younathan, J.; Meyer, T. J. *Coord. Chem. Rev.* **1991**, *111*, 47.
(32) Nelson, R. D.; Lide, D. R.; Maryott, A. A. *Selected Values of Electric Dipole Moments for Molecules in the Gas Phase*; National Standards References Data Series 10; National Bureau of Standards: Washington, DC, 1967.
(33) Stuart, H. A. In *Landolt-Borstein Zahlenwerte and Funktionen*, Eucken, A., Kellwege, K. H., Eds., Springer-Verlag, Berlin, 1951, Part 3, Vol. 1, pp 511−513.

(34) LeFevre, C. G.; LeFevre, R. J. W.; Rao, B. P.; Smith, M. R. *J. Chem. Soc*. **1959**, 1188.
(35) Sanyal, N. K.; Ahmad, P.; Dixit, L. *J. Phys. Chem*. **1973**, *77*, 2552.
(36) Adams, S.; Nir, S.; Rein, R. *Int. J. Quantum Chem.* **1975**, *9*, 701.
(37) No, K. T.; Cho, K. H.; Jhon, M. S.; Scheraga, H. A. *J. Am. Chem. Soc*. **1993**, *115*, 2005.
(38) Rodgers, M. T.; Ervin, K. M.; Armentrout, P. B. *J. Chem. Phys*. **1997**, *106*, 4499.
(39) Rodgers, M. T. *J. Phys. Chem. A* **2001**, *105*, 2374.
(40) Teloy, E.; Gerlich, D. *Chem. Phys*. **1974**, *4*, 417.
(41) Gerlich, D. *Adv. Chem. Phys*. **1992**, *82*, 1.
(42) Ervin, K. M.; Armentrout, P. B. *J. Chem. Phys*. **1985**, *83*, 166.
(43) Dalleska, N. F.; Honma, K.; Sunderlin, L. S.; Armentrout, P. B. *J. Am. Chem. Soc*. **1994**, *116*, 3519.
(44) Becke, A. D. *J. Chem. Phys.* **1993**, *98*, 5648.
(45) Lee, C.; Yang, W.; Parr, R. G. *Phys. Rev. B* **1988**, *37*, 785.
(46) Foresman, J. B.; Frisch, A. E. *Exploring Chemistry with Electronic Structure Methods*, 2nd ed.; Gaussian: Pittsburgh, 1996; p 64.
(47) Boys, S. F.; Bernardi, R. *Mol. Phys*. **1979**, *19*, 553.
(48) van Duijneveldt, F. B.; van Duijneveldt, V. R.; Van, Lenthe, J. G. C. M. *Chem. Rev.* **1994**, *94*, 1873.
(49) Smith, S. M.; Markevitch, A. N.; Romanor, D. A.; Li, X.; Levis, R. J.; Schlegel, H. B. *J. Phys. Chem. A* **2000**, *108*, 11063.
(50) Glendening, E. D.; Badenhoop, J. K.; Reed, A. E.; Carpenter, J. E.; Weinhold, F. *NBO*, Version 3.1; University of Wisconsin: Madison, 1995.
(51) Muntean, F.; Armentrout, P. B. *J. Chem. Phys.* **2001**, *115*, 1213.
(52) Beyer, T. S.; Swinehart, D. F. *Comm. Assoc. Comput. Mach.* **1973**, *58*, 2438.
(53) Khan, F. A.; Clemmer, D. E.; Armentrout, P. B. *J. Phys. Chem.* **1993**, *113*, 7978.
(54) Armentrout, P. B.; Simons, J. *J. Am. Chem. Soc*. **1992**, *114*, 8627.
(55) Rodgers, M. T.; Armentrout, P. B. *Mass Spectrom. Rev*. **2000**, *19*, 215.
(56) Amunugama, R.; Rodgers, M. T. *J. Phys. Chem. A* **2001**, *105*, 9883.
(57) Rodgers, M. T.; Armentrout, P. B. *J. Phys. Chem. A* **1999**, *103*, 4955.
(58) Weber, M. E.; Elkind, J. L.; Armentrout, P. B. *J. Chem. Phys*. **1986**, *84*, 1521.
(59) Miller, K. J. *J. Am. Chem. Soc*. **1990**, *112*, 8533.
(60) Rodgers, M. T.; Stanley, J. R.; Amunugama, R. *J. Am. Chem. Soc.* **2000**, *122*, 10969.
(61) Amunugama, R.; Rodgers, M. T. *Int. J. Mass. Spectrom*. **2000**, *195/196*, 439.
(62) Rodgers, M. T.; Armentrout, P. B. *Int. J. Mass. Spectrom.* **1999**, *185/186/187*, 359.
(63) Rannulu, N. S.; Amunugama, R.; Yang, Z.; Rodgers, M. T. *J. Phys. Chem. A* **2004**, *108*, 6385.
(64) McKenna, A. G.; McKenna, J. F. *J. Chem. Educ*. **1984**, *61*, 771.
(65) Rannulu, N. S.; Rodgers, M. T. *Phys. Chem. Chem. Phys.* **2005**, *7*, 1014.
(66) Yang, Y. S.; Hsu, W. Y.; Lee, H. F.; Huang, Y. C.; Yeh, C. S.; Hu, C. H. *J. Phys. Chem. A* **1999**, *103*, 11287.
(67) Chu, Y.; Yang, Z.; Rodgers, M. T. *J. Am. Soc. Mass Spectrom*. **2002**, *13*, 453.
(68) Vitale, G.; Valina, A. B.; Huang, H.; Amunugama, R.; Rodgers, M. T. *J. Phys. Chem. A* **2001**, *105*, 11351.
(69) Walter, D.; Armentrout, P. B. *J. Am. Chem. Soc*. **1998**, *120*, 3176.
(70) Koizumi, H.; Zhang, X. G.; Armentrout, P. B. *J. Phys. Chem. A* **2001**, *105*, 2444.
(71) Bauschlicher, C. W.; Langhoff, S. R.; Partridge, H. *J. Chem. Phys.* **1991**, *94*, 2064.
(72) Bauschlicher, C. W.; Langhoff, S. R.; Partridge, H. *J. Phys. Chem*. **1992**, *96*, 3273.
(73) Langhoff, S. R.; Bauschlicher, C. W.; Partridge, H. *J. Phys. Chem.* **1991**, *95*, 10667.